NF κ B-Induced Periostin Activates Integrin- β 3 Signaling to Promote Renal Injury in GN

Niki Prakoura, Panagiotis Kavvadas, Rapha l Kormann, Jean-Claude Dussaule, Christos Chadjichristos, Christos Chatziantoniou

NFκB-Induced Periostin Activates Integrin-β3 Signaling to Promote Renal Injury in Glomerulonephritis

Niki Prakoura[1], Panagiotis Kavvadas[1], Raphaël Kormann[1,2], Jean-Claude Dussaule[1,2,3], Christos E. Chadjichristos[1,2] and Christos Chatziantoniou[1,2]

[1]Institut National de la Santé Et de la Recherche Médicale UMRS 1155, Tenon Hospital, Paris, France.

[2]Sorbonne Universités, UPMC Paris 6, Paris, France.

[3]Department of Physiology, Saint-Antoine Hospital, Assistance Publique-Hôpitaux de Paris, Paris, France.

Running title: Periostin targeting reverses CKD

Abstract word count: 200

Text word count: 2934

Correspondence:

Dr. Christos Chatziantoniou,

INSERM UMRS 1155, Tenon Hospital, 4 rue de la Chine, 75020 Paris, France.

Email: christos.chatziantoniou@upmc.fr

Tel: (331) 56016653, Fax: (331) 56016659

Abstract

De novo expression of periostin in the kidney, a protein involved in odonto- and osteogenesis, has been suggested as biomarker of renal disease. In this study, we present novel findings on the mechanism(s) of induction and the role of periostin in renal disease. Using combined bioinformatics, reporter-assay and chromatin immunoprecipitation analyses, we found that periostin is induced by pro-inflammatory transcription factors in glomeruli during experimental glomerulonephritis. This *de novo* expression of periostin is essential for the induction of integrin-β3 driving downstream activation of Focal Adhesion Kinase and AKT pathways to affect cell survival and motility promoting renal damage. Periostin increased the expression of integrin-β3 concomitant to phosphorylation of Focal Adhesion Kinase and AKT in podocytes *in vitro*. Animals lacking expression of periostin displayed preserved renal function and structure during glomerulonephritis. Furthermore, delayed administration of periostin antisense oligonucleotides in wt animals reversed the already established proteinuria, diminished tissue inflammation and improved renal structure. Interestingly, periostin and integrin-β3 were highly co-localized in biopsies from inflammatory glomerulonephritis. These results demonstrate that interplay between periostin and renal inflammation orchestrates inflammatory and fibrotic responses, driving podocyte damage through downstream activation of integrin-β3 signaling. Targeting periostin may be a novel therapeutic strategy against chronic kidney disease.

Introduction

Chronic kidney disease (CKD) is a major burden worldwide with currently no available early prognostic marker or efficient therapeutic treatment. Although various stimuli can lead to CKD, there are common mechanisms characterized by chronic inflammation and accumulation of extracellular matrix within the kidney, resulting in decline of renal function and finally end stage renal disease.

Periostin is a matricellular protein abundant in periosteum, periodontal ligament, bone, skin and developing heart.[1,2] Periostin interacts with extracellular matrix components including collagen I, tenascin-C and fibronectin, promoting collagen fibrilogenesis and increased strength performance of the extracellular matrix.[3-5] Interaction of periostin with cell-surface integrins avβ3 and avβ5 has been associated with increased adhesion and migration of cancer cells and vascular smooth muscle cells (SMCs).[6,7] Periostin is highly induced *in vitro* by TGF-β1,[1,5,8] while it was also found to be up-regulated by Angiotensin II in cardiac fibroblasts.[8] IL-4 and IL-13 increased periostin in lung fibroblasts and bronchial epithelial cells, associating its induction with asthma.[9]

Periostin has been found up-regulated in renal disease models and kidney biopsy specimens. It was found highly over-expressed in experimental polycystic kidney disease promoting cyst growth and fibrosis.[10] Periostin tissue expression and urinary levels were inversely correlated with renal function in lupus nephritis and type II diabetes patients, respectively.[11,12] Periostin mRNA expression was highly up-regulated in both glomeruli and tubulointerstitium in patients with different nephropathies.[13] We previously reported that periostin expression is highly correlated

with disease progression in a model of hypertensive nephropathy and we subsequently showed that mice lacking periostin are protected against the structural alterations induced by Unilateral Ureteral Obstruction.[14,15]

Despite these findings, the mechanisms of induction and function of periostin in renal disease are largely unknown. In the present study we investigated these mechanisms in an established chronic renal disease model induced by nephrotoxic serum (NTS) administration. We found that periostin is induced by key pro-inflammatory transcription factors with major being NFκB and showed that periostin co-localizes with integrin-β3 at sites of renal damage driving activation of phospho-FAK- and phospho-AKT-dependent pathways. Finally, using a pharmacogenetic approach of *in vivo* antisense administration after severe proteinuria and the disease onset, we showed that inhibition of periostin can be used as a therapeutic strategy to alleviate renal disease progression. Our findings describe for the first time how periostin is induced to mediate the progression of renal disease and underline periostin targeting as therapeutic treatment against CKD.

Results

Periostin is induced by pro-inflammatory transcription factors in the model of NTS-induced glomerulonephritis.

To find transcription factors that may induce periostin expression, we performed bioinformatics analysis of a 2kb region of periostin promoter using the Genomatix software. We focused on known pro-inflammatory and pro-fibrotic transcription factors and mapped their predicted binding sites on periostin promoter sequence (Figure 1A).

To examine the efficiency of these transcription factors to affect periostin expression, we performed luciferase assays using 2kb and 1kb constructs of human or mouse periostin promoter, together with expression plasmids of these transcription factors. The large subunit of NFκB, p65, highly induced the activity of both human periostin promoter constructs and even more impressively that of mouse promoter constructs (Figure 1B). Other pro-inflammatory transcription factors (c-Jun, Stat1a, Stat6) induced a two-fold increase in the activity of both human and mouse constructs (Figure 1C). In contrast, from the group of pro-fibrotic transcription factors, only Smad4 induced a sustained two-fold promoter activity with Smad3 and Smad5 resulting in a much smaller induction of promoter activity (Figure 1D). The increase of periostin mRNA paralleled the promoter activation after transfection with the transcription factor plasmids, confirming the results of the luciferase assay (Figure 1E).

We performed ChIP experiments to verify the *in vivo* binding of these transcription factors on periostin promoter in a chronic renal disease model, the NTS-induced glomerulonephritis. Indeed, p65 was highly enriched on its respective binding sites on periostin promoter after NTS administration (Figure 1F). Phospho-c-Jun and phospho-Stat1 were also enriched on several of their predicted binding sites on periostin promoter in the NTS group (Figure 1G-1H). On the contrary, phospho-Smad3 was not enriched on periostin promoter after NTS, in agreement with its low efficiency to induce periostin promoter activity or mRNA expression (Figure 1I).

Genetic deletion of periostin preserves renal structure and function in the NTS model.

We used periostin null mice in the C57BL/6 background and confirmed whether periostin expression was induced after NTS administration. Transcriptional and protein analysis showed increased renal expression of periostin in WT NTS mice compared with control littermates treated with PBS, while KO mice did not display any periostin expression (Figure 2A-2B). Next, we analyzed functional and structural alterations indicative of disease progression. The increase in weight caused by edema and the severe increase of proteinuria were markedly attenuated in KO mice, showing that lack of periostin resulted in preservation of kidney function (Figure 2C-2D). Histological examination of kidney sections stained with Masson's Trichrome showed that mice lacking periostin developed less fibrotic lesions and had highly preserved kidney structure together with decreased number of injured glomeruli (Figure 2E-2F).

We next examined the expression of known pro-inflammatory mediators and fibrotic molecules, as well as the inflammatory cell infiltration profile of the diseased kidneys. Both collagens I and III and pro-fibrotic TGF-β1 were up-regulated in WT NTS mice, but their expression was highly attenuated in KO mice (Figure 2G-2I). In parallel, the induction of pro-inflammatory mediators such as MCP-1, Rantes and VCAM-1 in WT mice after NTS was completely blunted in mice lacking periostin (Figure 2J-2L). Infiltration of macrophages and lymphocytes was markedly reduced in KO NTS mice (Figure 2M-2N), establishing a close connection between periostin and inflammation probably leading to development of fibrosis and renal damage.

Delayed inhibition of periostin prevents the development of renal disease in the NTS model.

To assess whether inhibition of periostin can be used as therapeutic approach in renal disease, we inhibited periostin expression via constant administration of antisense oligonucleotides (ODN) after induction of glomerulonephritis, while scrambled non-specific ODN was used as control.

Antisense administration in NTS mice efficiently inhibited the mRNA and protein up-regulation of periostin (Figure 3A-3B). The renal function of NTS scrambled mice was largely compromised, characterized by high increase in weight, proteinuria and BUN levels. These changes were reversed in mice receiving antisense: body weight and BUN increases were blunted and proteinuria was decreased to almost control levels (Figure 3C-3E). Treatment with antisense against periostin resulted in better preservation of kidney structure characterized by restricted formation of fibrotic, glomerular and tubular lesions compared to severe structural alterations in NTS scrambled mice (Figure 3F-3H). The preservation of kidney structure and function in antisense-treated mice was accompanied by decreased expressions of pro-fibrotic (COL1, COL3, TGF-β1) and pro-inflammatory mediators (MCP-1, VCAM-1, CSF-1) (Figure 3I-3N), and by lesser infiltration of macrophages and lymphocytes compared to NTS scrambled mice (Figure 3O-3P).

Periostin is co-localized with integrin-β3 at sites of renal damage and drives integrin-β3 downstream signaling.

We performed immunohistochemical analysis to localize periostin expression in the diseased kidney. In both NTS protocols, periostin showed a basic expression in

control vessels and a high up-regulation in vessels and injured glomeruli of damaged kidneys. Periostin expression was null in KO kidneys and highly diminished in antisense-treated kidneys (Figure 4A and 4D). Interestingly, integrin-β3, a proposed periostin receptor, was *de novo* expressed in NTS mice, with its expression being nearly blunted in KO or antisense-treated mice (Figure 4B and 4E) and was also localized in vessels and glomeruli of damaged kidneys (Figure 4C and 4F). Staining of serial sections verified that integrin-β3 and periostin were co-expressed at the same sites in diseased kidneys (Figure 4G). Further double co-staining with nestin or CD44 showed that both proteins are over-expressed in podocytes and activated parietal epithelial cells in the NTS model (Figure 4H-4I). On the contrary, co-staining of periostin with α-SMA or CD146 did not reveal any co-localization with glomerular mesangial or endothelial cells, respectively (Figure 4I). Notably, co-immunoprecipitation analysis demonstrated that periostin interacts with its receptor, integrin-β3, *in vivo* during development of renal disease (Figure 4J).

To further investigate the connection between periostin and integrin-β3, we analyzed the expression of known mediators of integrin-β3 downstream signaling in the NTS model. We found that p-FAK, known for mediating cell adhesion and motility, was induced several-fold in WT mice after NTS, whereas its expression remained low in the KO NTS group (Figure 5A). Similarly, p-AKT, a mediator of cell survival and growth, was *de novo* expressed in renal vessels and glomeruli following NTS, while its expression was negligible in KO kidneys (Figure 5B). Co-staining with CD44 and nestin revealed that both integrin mediators, p-FAK and p-AKT, were expressed by activated parietal cells and podocytes after NTS (Figure 5C), as was shown with periostin and integrin-β3 (Figure 4H-I).

To examine whether periostin is able to activate integrin-β3 and its downstream signaling, we incubated an immortalized podocyte cell line, one of the cell types being injured in the NTS model, with recombinant periostin. In a time-course experiment, periostin strongly induced the expression of integrin-β3 along with its effectors p-FAK and p-AKT with a peak at 6 h (Figure 5D-5E).

Periostin and integrin-β3 co-localize in renal biopsies.

To investigate whether periostin and integrin-β3 are co-expressed in cases of human renal disease, we performed immunohistochemical localization of both proteins in consecutive sections of renal biopsies from patients with ANCA Vasculitis, an inflammatory glomerulopathy. A strong staining for both periostin and integrin-β3 was observed in the examined biopsies, and the proteins were found to co-localize within damaged glomeruli and tubules (Figure 6). In addition, a comparison of gene expression profiles from renal disease datasets deposited in the publicly available platform Nephroseq revealed a strong correlation and a comparable up-regulation of periostin and integrin-β3 in several of these datasets (Supplemental Figure 1). These results support the notion that periostin and integrin-β3 cooperate to mediate the development of renal disease.

Discussion

The increasing prevalence of CKD and the lack of efficient treatment necessitate the discovery of novel prognostic markers and therapeutic targets. Periostin, a matricellular protein associated with mesenchymal phenotype and fibrous structures, was found by us and other investigators to be highly induced in the kidney in several types of renal disease, both in animal models and patient biopsies.[16,17] Nevertheless, the mechanism(s) of induction and the actual role of periostin during disease progression have not been examined. The present study aimed to unravel these mechanisms in an established model of NTS-induced renal disease. Our results showed for the first time that pro-inflammatory transcription factors induce periostin in renal disease. Moreover, periostin was found to drive both the expression and downstream signaling of integrin-β3, a proposed periostin receptor, causing phenotypical changes associated with disease progression. Finally, we showed that delayed *in vivo* inhibition of periostin after the disease onset can efficiently alleviate the progression of severe renal disease. The proposed mechanisms of induction and function of periostin in renal disease are summarized in Figure 7.

Little is presently known about the transcription factors that control periostin gene expression. Twist was shown to bind and induce periostin promoter activity in preosteoblasts, while YY1 was found to bind on a conserved enhancer region on periostin promoter, regulating tissue-specific periostin expression in the cardiac cushion mesenchyme.[18,19] Our bioinformatics analysis revealed the presence of several putative pro-inflammatory transcription factor binding sites on periostin promoter, while transcription factor binding sites of the classical TGF-β1 signaling pathway which has been shown to up-regulate periostin *in vitro*,[1,5,8] were very rare. In

luciferase-assays and at the endogenous gene level we showed that key pro-inflammatory transcription factors including NFκB (p65), c-Jun and STAT1 directly induced periostin promoter activity or gene expression, respectively. The active forms of these transcription factors were found to be highly enriched *in vivo* on periostin promoter in NTS-induced glomerulonephritis, indicating that periostin was up-regulated in response to these transcription factors in the NTS model. The fact that phopho-Smad3 was not enriched on periostin promoter implies that either periostin is not induced by TGF-β1 in the NTS model or that TGF-β1 may control periostin expression by a Smad-independent pathway, involving the activation of pro-inflammatory transcription factors like NFκB, Jun and STAT.[20]

The induction of periostin by pro-inflammatory pathways correlates with its observed role to promote inflammatory reactions in several disease contexts. In allergen-induced skin inflammation, IL-4 and IL-13 were shown to induce periostin which further amplified Th-2 type immune responses.[21] Besides, periostin-deficient lung fibroblasts showed lower production of chemokines in response to TNF-α, accounting for the lack of inflammatory response in pulmonary fibrosis.[22] In a model of glioblastoma xenografts, periostin secreted by stem cells was found to recruit tumor-associated macrophages promoting malignant growth.[23] These studies are in accordance with our observations that lack or inhibition of periostin reduced the production of pro-inflammatory cytokines and the subsequent macrophage and lymphocyte infiltration in the injured kidneys. To examine whether the difference in the inflammatory response was due to strain difference in the activation of inflammatory cells, we compared the activated monocytes/macrophages of WT and KO mice after thioglycolate-induced peritonitis. Numeration of the infiltrated

peritoneal monocytes after thioglycolate treatment did not show any differences between WT and KO mice (Supplemental Figure 2A). Leukocyte cell analysis before and after thioglycolate treatment did not reveal any variations in the leukocyte subtypes (Supplemental Figure 2B). In migration assays towards chemoattractant MCP-1, the isolated peritoneal monocytes of WT and KO mice showed the same migratory capacities, also explained by the similar expression levels of various receptors and cytokines (Supplemental Figure 2C-2D). Notably, periostin expression was null in the isolated WT monocytes. Thus, periostin expression by the damaged renal tissue is crucial in inducing production of chemokines to attract inflammatory cells at the sites of injury. Accordingly, recombinant periostin was found to directly enhance adhesion of eosinophils and monocytes to fibronectin and function as chemoattractant to primary monocytes and macrophages in migration assays.[24,25]

Chronic inflammation plays a central role in development of fibrosis and kidney damage. Concomitantly to the attenuation of inflammation, periostin deficiency diminished the expression of collagens, TGF-β1 and improved renal structure and function. Periostin has been associated with fibrosis in several tissues. Analysis of periostin expression in human skin pathologies demonstrated that it is over-expressed during scar formation, associated with wound healing and pathological remodeling.[26] Accordingly, periostin null dermal fibroblasts showed reduced expression of *Acta2* and *Col1a1* transcripts upon TGF-β1 treatment,[27] while mesenchymal cells treated with exogenous periostin showed increased collagen production and wound closure.[28] In a model of acute myocardial infarction, periostin null mice exhibited impaired cardiac healing as a result of reduced myocardial stiffness and collagen fibril formation, while inducible over-expression of periostin protected mice from cardiac

rupture.[29,30] The ability of periostin to interact and stabilize fibrilar collagens and other extracellular matrix molecules is probably a key event by which periostin controls extracellular matrix deposition and development of fibrosis.[3-5]

We found *de novo* expressed periostin to co-localize and interact with integrin-β3 in glomeruli and vascular SMCs of NTS mice. Over-expression of periostin in aortic SMCs induced migration together with increased integrin-β3 expression and FAK phosphorylation.[7] In addition, periostin expression was increased in vascular SMCs subjected to mechanical strain, and this increase was followed by FAK activation and MCP-1 secretion, which were inhibited by a periostin-neutralizing antibody.[31] In agreement with these studies, induction of periostin in the NTS model was determinant for the *de novo* expression of integrin-β3 followed by downstream FAK and AKT activation. Thus, periostin may induce and activate integrin-β3 promoting motility, permeability and secretion of chemokines essential for remodeling and inflammatory cell infiltration.[32]

Activation of integrin avβ3 in podocytes has been shown to mediate podocyte dysfunction, motility and proteinuria in focal segmental glomerulosclerosis and LPS-induced renal disease.[33,34] In the NTS model, induction of integrin-β3 and its downstream signaling in parietal cells and podocytes was dependent on the expression of periostin. Treatment of cultured podocytes with recombinant periostin was sufficient to increase integrin-β3 expression followed by FAK and AKT activation. Activation of FAK and AKT in the injured podocytes and activated parietal cells induces cell motility, invasion,[35] and crosstalk between the two glomerular cell types, resulting ultimately in foot process effacement, proteinuria and kidney damage.

We found strong expression and high degree of co-localization between periostin and integrin-β3 in renal biopsies from ANCA vasculitis patients. In addition to their glomerular expression, both proteins were also localized in tubular cells in the human biopsies. This difference with the NTS model may reflect the distinct stimuli causing the disease, which in the case of the NTS model target primarily the glomerulus, while in the case of ANCA vasculitis affect the whole kidney. To further investigate the co-expression pattern of periostin and integrin-β3 in renal disease patients, we performed a meta-analysis of gene expression profiles from renal disease datasets deposited in the Nephroseq platform (www.nephroseq.org). We compared the expression levels of periostin and integrin-β3 in a similar disease dataset as the biopsies used in our study (vasculitis patients vs. healthy donors, n=52), and found a strong correlation between periostin and integrin-β3 (R=0.544, p<0.0001). Moreover, both proteins were significantly up-regulated to a comparable level in several other datasets (Supplemental Figure 1).

Presently, only two studies in animal models of pulmonary fibrosis and ovarian cancer have shown that inhibition of periostin via blocking antibodies could be used as a therapy against the disease progression.[28,36] We used an alternative strategy of *in vivo* antisense administration after establishment of severe proteinuria and found that inhibition of periostin could remarkably diminish the inflammation and reverse the increase in proteinuria. The ability of periostin to play distinctive roles in crucial events during development of renal disease by promoting tissue inflammatory response, accumulation of extracellular matrix and podocyte damage underline periostin targeting as a potential efficient future treatment against CKD.

Concise Methods

Immunohistochemical staining of patient biopsies

All procedures and use of human tissue were performed according to the national ethical guidelines and were in accordance with the Declaration of Helsinki. Written informed consent was given by the patients for use of part of their biopsy for scientific purposes prior to inclusion in the study.

Renal biopsies from patients were retrospectively analyzed. Experiments were performed on biopsies from patients with ANCA Vasculitis. The biopsies were characterized by diffuse glomerular lesions, fibrin deposits, weak lesions of acute tubular necrosis and extra-capillary crescentic proliferation. 4-µm formalin-fixed, paraffin-embedded consecutive kidney sections were stained with primary antibodies for periostin (Abcam ab14041) or integrin-β3 (Abcam ab75872). Appropriate secondary antibodies (N-Histofine, Nichirei Biosciences) and AEC (Dako) as substrate were used. Slides were counterstained with hematoxylin QS (Vector) and mounted with permanent aqueous mounting medium (ScyTek). A total of four patient's biopsies were used for this set of experiments.

Animal models

All procedures regarding animal experimentation were in accordance with the European Union Guidelines for the Care and Use of Laboratory Animals and approved by the local ethics committee of the National Institute for Health and Medical Research (INSERM). Animals were housed at constant temperature with free access to water and food.

The strain of periostin KO mice was created at the laboratory of Dr. Simon Conway and has been previously described.[15] For the model of NTS-induced

glomerulonephritis, decomplemented NTS was prepared as previously described.[37-38] Female WT and KO littermate mice of the C57BL/6 background aged 8-10 weeks received intravenous injections of totally 15 μl NTS/gr body weight over 2 consecutive days (days 0 and 1) to induce crescentic glomerulonephritis. Control mice were injected with PBS. Mice were euthanized 14 days after the first injection (*n*= 6-7 per group). Blood, urine, and renal tissues were collected for subsequent analyses.

For the antisense experiments, SV129 male WT mice aged 8-10 weeks were used. The mice received intravenous injections of totally 12 μl NTS/gr body weight over 2 consecutive days (days 0 and 1) to induce crescentic glomerulonephritis, while control mice were injected with PBS. Periostin expression was inhibited with a cocktail of two different ODNs specifically targeting periostin mRNA, designed using IDT (Integrated DNA Technologies) platform, also previously described (15). Scrambled non-specific ODNs were used as control. The ODN sequences were modified with phosphorothioate to prevent their in vivo hydrolysis by nucleases (Sigma-Aldrich, Supplemental Table 1). For administration to mice, the ODNs were diluted in normal saline and placed in osmotic mini-pumps (Alzet, model 1002) which were subsequently implanted subcutaneously in mice, constantly releasing a dose of 0.25 μl/hr which corresponded to a release of 150 pmol/ODN/day. The implantation of mini-pumps was performed at day 3 after administration of NTS, taking one day for the pump to start functioning. Mice were euthanized 9 days after the first injection (*n*= 5 per group). Blood, urine, and renal tissues were collected.

Proteinuria and BUN Measurements

Urine was collected at several time points during the mouse protocols, while blood was collected at the end of each protocol. Proteinuria was measured using a Konelab

analyzer (Thermo Fisher Scientific), and was normalized to urine creatinine. BUN levels were measured with an enzymatic method (Konelab analyzer) and expressed in millimoles per liter.

Histological Evaluation

Formalin-fixed, paraffin-embedded, 4-µm thick kidney sections were stained with Masson's Trichrome. Quantifications were performed by examining at least 10 microphotographs of random, non-overlapping fields at 200x magnification per mouse. Crescents, fibrin deposits and glomerulosclerosis were expressed as percentage of the total glomeruli evaluated. Tubular dilation was examined using a 0 (no dilation) to 3 (high dilation) injury scale per photograph and the mean value was calculated for each mouse.

The evaluation of glomerular injury on the resistant C57BL/6 background was based on the combined examination of mesangial matrix expansion, endothelial wall thickening, capillary rupture and glomerular infiltration and was expressed as percentage of injured glomeruli per total glomeruli examined.

Western Blot Analysis

Proteins from half kidneys or cell culture were extracted in a commercial RIPA lysis buffer supplemented with PMSF, a protease inhibitor cocktail and sodium orthovanadate (Santa Cruz) and total protein concentration was measured using the Bradford assay. Equal amounts of proteins were loaded on a NuPAGE 4-12% gradient gel (Invitrogen) and transferred to nitrocellulose membrane (Biorad). Immunoblotting was performed for periostin (R&D Systems, MOSF20), integrin-β3 (Abcam ab75872), pFAK (Cell Signaling #3283), FAK (Santa Cruz sc-557), pAKT

(Cell Signaling #9271), AKT 1/2/3 (Santa Cruz sc-8312). Gapdh (Sigma) was used as loading control.

Quantitative Real-time PCR

Total RNA was extracted from half kidneys using TRI Reagent (MRC) and from cell cultures using the EZ-10 Spin Column Total RNA Mini-preps Super kit (Bio Basic Inc). RNA quality was verified by measuring the OD 260/280 ratio and residual genomic DNA was removed by DNase I treatment (Thermo Scientific) for 30minutes at 37°C. 1µg RNA was transcribed to cDNA using the Maxima First Strand cDNA Synthesis Kit from Thermo Scientific according to manufacturer's instructions. Real-time PCR was performed with the Roche Light Cycler 480® detection system using SYBR Green PCR Master Mix (Roche). Specific primers for target mRNAs (Supplemental Table 2) were used for amplification under the following program: 95°C for 5 minutes, 45 cycles at 95°C for 15 seconds and 60°C for 15 seconds, and 72°C for 15 seconds. For quantitative analysis, experimental genes were normalized to *Gusb* mRNA or *Hprt* mRNA expression using the ΔΔCT method. Dissociation curves were analyzed in order to determine that a single product was amplified.

Immunohistochemistry and double immunofluorescence

For immunostaining of macrophages and lymphocytes, 4-µm formalin-fixed, paraffin-embedded kidney sections were stained with primary antibodies to F4/80 (MCA497R Abd Serotec) or CD3 (Dako A0452) respectively. Appropriate secondary antibodies (N-Histofine, Nichirei Biosciences) and AEC (Dako) as substrate were used. Slides were counterstained with hematoxylin QS (Vector) and mounted with permanent aqueous mounting medium (ScyTek). The F4/80 and CD3 positive area was

quantified in at least 10 photographs at 200x magnification per animal, using publicly available image processing software (Image J Fiji), and expressed as percentage of the total tissue area.

For periostin immunostaining, 5-µm frozen tissue sections were fixed in 4% PFA for 15 min, blocked in 10% FBS and incubated with primary anti-periostin antibody (Thermo Scientific PA5-34641). For integrin-β3 and pAKT immunostaining, the following antibodies for integrin-β3 (Abcam ab75872) and pAKT (Abcam ab81283) on 4-µm formalin-fixed, paraffin-embedded kidney sections were used. Incubation with secondary antibodies and signal detection was performed as described above.

Dual immunolabeling was performed on 5-µm frozen or 4-µm paraffin tissue sections incubated with primary antibodies to periostin, integrin-β3, nestin (BD Pharmingen 556309), CD44 (Exbio 11-624-C100), α-SMA (Sigma A5228), CD146 (kind gift), pAKT and pFAK (Abcam ab55335). The signal was detected with Alexa Fluor secondary antibodies followed by DAPI counterstain and mounting in PermaFluor medium (Thermo Scientific).

E11 podocyte cell culture

The E11 immortalized mouse podocyte cell line was cultured as previously described (17). Briefly, cells were maintained in RPMI 1640 medium supplemented with 10% FBS, 100 U/ml penicillin-streptomycin, and 10 U/mL recombinant mouse INFγ (Peprotech) to induce synthesis of the immortalizing T antigen at 33°C/5% CO_2. To initiate differentiation, cells were trypsinized and thermoshifted to 37°C in medium without INFγ for 10-15 days. For treatment with recombinant mouse periostin, differentiated cells in 6-well plates were serum starved for 24 hrs and incubated with

recombinant periostin (R&D Systems) at a concentration of 400 or 1000 ng/ml for the indicated time points.

Cell culture and transfection

HEK293 cell line was maintained in DMEM 4.5 g/l glucose supplemented with 10% FBS, 100 U/ml penicillin-streptomycin and 2mM L-glutamine at 37°C/5% CO_2. Transfection was performed in 12-well plates via the $CaCl_2$ method. Briefly, 2 hrs before transfection cells were replenished with fresh culture medium. Each well was transfected with a mixture of 0.35μg pGL3 plasmid, 0.35μg CMV-β-gal plasmid (used for normalization) and 1.25μg transcription factor expression plasmid added to 14μl 2M CaCl2 and 111μl 2x HBS solution (Sigma) in a final volume of 222μl. The day after transfection cell medium was replaced with fresh medium and the cells were incubated for another day before being tested in the luciferase assay or subjected to RNA extraction followed by QRT-PCR.

Plasmid construction

The pGL3-basic luciferase reporter vector (Promega), the CMV-β-gal expression plasmid and the expression plasmids for Smad3, Smad4 and Smad5 were kindly provided by Dr. A. Charonis (Biomedical Research Foundation of the Academy of Athens). Expression plasmids for RelA/p65 (#21984), c-Jun (#47443), Stat1a (#8690) and Stat6 (#35482) were obtained from Addgene. PUC19 encoding for an inactive fragment of β-galactosidase was used as control plasmid for transfection. The human and mouse periostin promoter regions hProm 2kb (-2003+113), hProm 1kb (-888+113), mProm 2kb (-2037+20) and mProm 1kb (-876+20), taking +1 as the transcription start site (TSS), were amplified by PCR from human or mouse DNA and

cloned into the multiple cloning site (MCS) sequence of pGL3-basic vector. The translation start site (ATG) for human periostin gene is at +119 and for mouse periostin gene is at +35 after TSS.

Bioinformatics analysis

Bioinformatics analysis of human and mouse periostin promoters was performed by the Genomatix software (www.genomatix.de). The desired promoter sequence was retrieved by the genomatix database using the tool Gene2Promoter followed by multiple alignment to check for conserved sequences and detection of putative transcription factor binding sites according to sequence similarity.

Luciferase assays

For luciferase activity measurement, the Luciferase Assay System from Promega (E4030) was used according to manufacturer's instructions. Briefly, the cells were lysed in Reporter Lysis Buffer (RLB), the extract was collected after centrifugation and removal of cell debris and luciferase activity was measured immediately in a luminometer after mixing 15µl extract with 70µl Luciferase Assay Reagent. To normalize luciferase measurements, the activity of β-galactosidase was measured in a β-gal assay. For each sample, 30µl cell extract were mixed with 3µl Magnesium solution (0.1M $MgCl_2$, 4.5M β-mercaptoethanol), 66µl ONPG (substrate) and 201µl sodium phosphate (pH 7.5) and incubated at 37^{o}C for few minutes until the development of a faint yellow color. The reaction was stopped by addition of 1M Na_2CO_3 and absorbance was measured against blank at 420nm. The results were expressed as ratio of the relative luciferase units (RLU) to β-gal measurements.

Chromatin Immunoprecipitation (ChIP)

ChIP was performed in kidneys from WT SV129 mice injected with NTS or PBS (control), using the SimpleChIP® Plus Enzymatic Chromatin IP Kit (#9005) from Cell Signaling according to manufacturer's instructions. Briefly, whole kidneys were finely minced and cross-linked with 1.5% formaldehyde for 20 min under constant rotation, followed by addition of 0.1M glycine to stop the reaction. The tissue was disaggregated using a dounce homogenizer, nuclei were prepared and chromatin was digested, sonicated and analyzed by gel electrophoresis and OD_{260} measurement to determine DNA concentration. Precipitation was performed with ChIP-graded antibodies from Cell Signaling: NF-κB p65 (#8242), p-c-Jun (#3270), p-Stat1 (#7649), p-Smad3 (#9520). Rabbit IgG was used as control. The precipitated complexes were purified with the use of Protein G Magnetic Beads, cross-links were reversed and DNA was eluted and purified. Sequence-specific primers for selected regions of mouse periostin promoter (Supplemental Table 3) were used in subsequent quantitative Real-time PCR analysis in order to check for enrichment of precipitated DNAs in the NTS over the PBS group. The results were expressed as percentage of the Input (total DNA used for immunoprecipitation).

Co-Immunoprecipitation (co-IP)

Protein interactions were stabilized by crosslinking minced half kidneys with DTSSP (Thermo Scientific #21578) according to manufacturer's instructions. Proteins were extracted in Pierce IP lysis buffer (#87787) supplemented with PMSF, a protease inhibitor cocktail and sodium orthovanadate and total protein concentration was measured using the Bradford assay. Equal amounts of proteins were precipitated with a rabbit anti-integrin-β3 antibody (Abcam ab119992) and rabbit IgG was used as

control. The precipitated complexes were purified with the use of Protein G Magnetic Beads (Cell Signaling #8740) and loaded on a denaturating SDS-PAGE followed by Western Blot. Equal amounts of Input were also loaded on the same gel. Immunoblotting was performed for periostin (R&D Systems, MOSF20) and the membrane was stripped using Restore™ Western Blot Stripping Buffer (Thermo Scientific #21059) and re-blotted for integrin-β3 (Abcam ab75872) and Gapdh (Sigma). Veriblot for IP secondary antibody (Abcam ab131366) detecting preferentially the non-reduced form of the IgG was used, in order to avoid non-specific signal from co-eluted reduced forms of the antibodies used for IP.

Statistical analysis

Data are expressed as mean values +/- SEM. Data were analyzed using one-way ANOVA followed by a Fisher's test. Values of $p<0.05$ were considered significant.

Acknowledgements

We are thankful to Dr. Aristidis Charonis and Dr. Panagiotis Politis (from Biomedical Research Foundation of the Academy of Athens) for providing plasmid expression vectors. We would also like to thank Dr. Nicole Endlich for providing the podocyte cell line and Caroline Martin for valuable help with animal breading. CD146 antibody was a generous gift from Pr. Françoise Dignat-George.

This work was supported by grants from INSERM. N.P. was recipient of a long-term fellowship from the society of European Renal Association-European Dialysis and Transplantation (ERA-EDTA).

Statement of competing financial interests

The authors have declared that no conflict of interest exists.

References

1. Horiuchi K, Amizuka N, Takeshita S, Takamatsu H, Katsuura M, Ozawa H, Toyama Y, Bonewald LF, Kudo A: Identification and characterization of a novel protein, periostin, with restricted expression to periosteum and periodontal ligament and increased expression by transforming growth factor beta. *J Bone Miner Res* 14: 1239–1249, 1999.

2. Kruzynska-Frejtag A, Machnicki M, Rogers R, Markwald RR, Conway SJ: Periostin (an osteoblast-specific factor) is expressed within the embryonic mouse heart during valve formation. *Mech Dev* 103: 183–188, 2001.

3. Norris RA, Damon B, Mironov V, Kasyanov V, Ramamurthi A, Moreno-Rodriguez R, Trusk T, Potts JD, Goodwin RL, Davis J, Hoffman S, Wen X, Sugi Y, Kern CB, Mjaatvedt CH, Turner DK, Oka T, Conway SJ, Molkentin JD, Forgacs G, Markwald RR: Periostin regulates collagen fibrillogenesis and the biomechanical properties of connective tissues. *J Cell Biochem* 101: 695-711, 2007.

4. Kii I, Nishiyama T, Li M, Matsumoto K, Saito M, Amizuka N, Kudo A: Incorporation of tenascin-C into the extracellular matrix by periostin underlies an extracellular meshwork architecture. *J Biol Chem* 285: 2028-2039, 2010.

5. Snider P, Hinton RB, Moreno-Rodriguez RA, Wang J, Rogers R, Lindsley A, Li F, Ingram DA, Menick D, Field L, Firulli AB, Molkentin JD, Markwald R, Conway SJ: Periostin is required for maturation and extracellular matrix stabilization of noncardiomyocyte lineages of the heart. *Circ Res* 102: 752-760, 2008.

6. Gillan L, Matei D, Fishman DA, Gerbin CS, Karlan BY, Chang DD: Periostin secreted by epithelial ovarian carcinoma is a ligand for alpha(V)beta(3) and alpha(V)beta(5) integrins and promotes cell motility. *Cancer Res* 62: 5358-5364, 2002.

7. Li G, Jin R, Norris RA, Zhang L, Yu S, Wu F, Markwald RR, Nanda A, Conway SJ, Smyth SS, Granger DN: Periostin mediates vascular smooth muscle cell migration through the integrins alphavbeta3 and alphavbeta5 and focal adhesion kinase (FAK) pathway. *Atherosclerosis* 208: 358-365, 2010.

8. Li L, Fan D, Wang C, Wang JY, Cui XB, Wu D, Zhou Y, Wu LL: Angiotensin II increases periostin expression via Ras/p38 MAPK/CREB and ERK1/2/TGF-β1 pathways in cardiac fibroblasts. *Cardiovasc Res* 91: 80-89, 2011.

9. Takayama G, Arima K, Kanaji T, Toda S, Tanaka H, Shoji S, McKenzie AN, Nagai H, Hotokebuchi T, Izuhara K: Periostin: a novel component of subepithelial fibrosis of bronchial asthma downstream of IL-4 and IL-13 signals. *J Allergy Clin Immunol* 118: 98-104, 2006.

10. Wallace DP, White C, Savinkova L, Nivens E, Reif GA, Pinto CS, Raman A, Parnell SC, Conway SJ, Fields TA: Periostin promotes renal cyst growth and interstitial fibrosis in polycystic kidney disease. *Kidney Int* 85: 845-854, 2014.

11. Wantanasiri P, Satirapoj B, Charoenpitakchai M, Aramwit P: Periostin: a novel tissue biomarker correlates with chronicity index and renal function in lupus nephritis patients. *Lupus* 24: 835-845, 2015.

12. Satirapoj B, Tassanasorn S, Charoenpitakchai M, Supasyndh O: Periostin as a tissue and urinary biomarker of renal injury in type 2 diabetes mellitus. *PLoS One* 10: e0124055, 2015.

13. Sen K, Lindenmeyer MT, Gaspert A, Eichinger F, Neusser MA, Kretzler M, Segerer S, Cohen CD: Periostin is induced in glomerular injury and expressed de novo in interstitial renal fibrosis. *Am J Pathol* 179: 1756-1767, 2011.

14. Guerrot D, Dussaule JC, Mael-Ainin M, Xu-Dubois YC, Rondeau E, Chatziantoniou C, Placier S: Identification of periostin as a critical marker of progression/reversal of hypertensive nephropathy. *PLoS One* 7: e31974, 2012.

15. Mael-Ainin M, Abed A, Conway SJ, Dussaule JC, Chatziantoniou C: Inhibition of periostin expression protects against the development of renal inflammation and fibrosis. *J Am Soc Nephrol* 25: 1724-1736, 2014.

16. Kavvadas P, Dussaule JC, Chatziantoniou C: Searching novel diagnostic markers and targets for therapy of CKD. *Kidney Int Suppl (2011)* 4: 53-57, 2014.

17. Prakoura N, Kavvadas P, Chatziantoniou C: New Targets for End-Stage Chronic Kidney Disease Therapy. *J Crit Care Med* 1: 92-95, 2015.

18. Oshima A, Tanabe H, Yan T, Lowe GN, Glackin CA, Kudo A: A novel mechanism for the regulation of osteoblast differentiation: transcription of periostin, a member of the fasciclin I family, is regulated by the bHLH transcription factor, twist. *J Cell Biochem* 86: 792-804, 2002.

19. Lindsley A, Snider P, Zhou H, Rogers R, Wang J, Olaopa M, Kruzynska-Frejtag A, Koushik SV, Lilly B, Burch JB, Firulli AB, Conway SJ: Identification and characterization of a novel Schwann and outflow tract endocardial cushion lineage-restricted periostin enhancer. *Dev Biol* 307: 340-355, 2007.

20. Moustakas A, Heldin CH: Non-Smad TGF-beta signals. *J Cell Sci* 118: 3573-3584, 2005.

21. Masuoka M, Shiraishi H, Ohta S, Suzuki S, Arima K, Aoki S, Toda S, Inagaki N, Kurihara Y, Hayashida S, Takeuchi S, Koike K, Ono J, Noshiro H, Furue M, Conway SJ, Narisawa Y, Izuhara K: Periostin promotes chronic allergic inflammation in response to Th2 cytokines. *J Clin Invest* 122: 2590-2600, 2012.

22. Uchida M, Shiraishi H, Ohta S, Arima K, Taniguchi K, Suzuki S, Okamoto M, Ahlfeld SK, Ohshima K, Kato S, Toda S, Sagara H, Aizawa H, Hoshino T, Conway SJ, Hayashi S, Izuhara K: Periostin, a matricellular protein, plays a role in the induction of chemokines in pulmonary fibrosis. *Am J Respir Cell Mol Biol* 46: 677-686, 2012.

23. W Zhou, SQ Ke, Z Huang, W Flavahan, X Fang, J Paul, L Wu, AE Sloan, RE McLendon, X Li, JN Rich, S Bao: Periostin secreted by glioblastoma stem cells recruits M2 tumour-associated macrophages and promotes malignant growth. *Nat Cell Biol* 17: 170-182, 2015.

24. Blanchard C, Mingler MK, McBride M, Putnam PE, Collins MH, Chang G, Stringer K, Abonia JP, Molkentin JD, Rothenberg ME: Periostin facilitates eosinophil tissue infiltration in allergic lung and esophageal responses. *Mucosal Immunol* 1: 289-296, 2008.

25. Arima M, Yoshida S, Nakama T, Ishikawa K, Nakao S, Yoshimura T, Asato R, Sassa Y, Kita T, Enaida H, Oshima Y, Matsuda A, Kudo A, Ishibashi T: Involvement of periostin in regression of hyaloidvascular system during ocular development. *Invest Ophthalmol Vis Sci* 53: 6495-6503, 2012.

26. Zhou HM, Wang J, Elliott C, Wen W, Hamilton DW, Conway SJ: Spatiotemporal expression of periostin during skin development and incisional wound healing: lessons for human fibrotic scar formation. *J Cell Commun Signal* 4: 99-107, 2010.

27. Yang L, Serada S, Fujimoto M, Terao M, Kotobuki Y, Kitaba S, Matsui S, Kudo A, Naka T, Murota H, Katayama I: Periostin facilitates skin sclerosis via PI3K/Akt dependent mechanism in a mouse model of scleroderma. *PLoS One* 7: e41994, 2012.

28. Naik PK, Bozyk PD, Bentley JK, Popova AP, Birch CM, Wilke CA, Fry CD, White ES, Sisson TH, Tayob N, Carnemolla B, Orecchia P, Flaherty KR, Hershenson

MB, Murray S, Martinez FJ, Moore BB; COMET Investigators: Periostin promotes fibrosis and predicts progression in patients with idiopathic pulmonary fibrosis. *Am J Physiol Lung Cell Mol Physiol* 303: L1046-1056, 2012.

29. Shimazaki M, Nakamura K, Kii I, Kashima T, Amizuka N, Li M, Saito M, Fukuda K, Nishiyama T, Kitajima S, Saga Y, Fukayama M, Sata M, Kudo A: Periostin is essential for cardiac healing after acute myocardial infarction. *J Exp Med* 205: 295-303, 2008.

30. Oka T, Xu J, Kaiser RA, Melendez J, Hambleton M, Sargent MA, Lorts A, Brunskill EW, Dorn GW 2nd, Conway SJ, Aronow BJ, Robbins J, Molkentin JD: Genetic manipulation of periostin expression reveals a role in cardiac hypertrophy and ventricular remodeling. *Circ Res* 101: 313-321, 2007.

31. Yamashita O, Yoshimura K, Nagasawa A, Ueda K, Morikage N, Ikeda Y, Hamano K: Periostin links mechanical strain to inflammation in abdominal aortic aneurysm. *PLoS One* 8: e79753, 2013.

32. Liu AY, Zheng H, Ouyang G: Periostin, a multifunctional matricellular protein in inflammatory and tumor microenvironments. *Matrix Biol* 37: 150-156, 2014.

33. Wei C, El Hindi S, Li J, Fornoni A, Goes N, Sageshima J, Maiguel D, Karumanchi SA, Yap HK, Saleem M, Zhang Q, Nikolic B, Chaudhuri A, Daftarian P, Salido E, Torres A, Salifu M, Sarwal MM, Schaefer F, Morath C, Schwenger V, Zeier M, Gupta V, Roth D, Rastaldi MP, Burke G, Ruiz P, Reiser J: Circulating urokinase receptor as a cause of focal segmental glomerulosclerosis. *Nat Med* 17: 952-960, 2011.

34. Wei C, Möller CC, Altintas MM, Li J, Schwarz K, Zacchigna S, Xie L, Henger A, Schmid H, Rastaldi MP, Cowan P, Kretzler M, Parrilla R, Bendayan M, Gupta V,

Nikolic B, Kalluri R, Carmeliet P, Mundel P, Reiser J: Modification of kidney barrier function by the urokinase receptor. *Nat Med* 14: 55-63, 2008.

35. Guo W, Giancotti FG: Integrin signalling during tumour progression. *Nat Rev Mol Cell Biol* 5: 816-826, 2004.

36. Zhu M, Saxton RE, Ramos L, Chang DD, Karlan BY, Gasson JC, Slamon DJ: Neutralizing monoclonal antibody to periostin inhibits ovarian tumor growth and metastasis. *Mol Cancer Ther* 10: 1500-1508, 2011.

37. Mesnard L, Keller AC, Michel ML, Vandermeersch S, Rafat C, Letavernier E, Tillet Y, Rondeau E, Leite-de-Moraes MC: Invariant natural killer T cells and TGF-beta attenuate anti-GBM glomerulonephritis. *J Am Soc Nephrol* 20: 1282–1292, 2009.

38. El Machhour F, Keuylian Z, Kavvadas P, Dussaule JC, Chatziantoniou C: Activation of Notch3 in Glomeruli Promotes the Development of Rapidly Progressive Renal Disease. *J Am Soc Nephrol* 26: 1561-1575, 2015.

Figure Legends

Figure 1. Periostin is up-regulated by pro-inflammatory transcription factors in the model of NTS-induced glomerulonephritis. (A) Mouse periostin promoter scheme with putative transcriptions factor binding sites, as resulted by bioinformatics analysis. (B to D) Luciferase-assay results in HEK293 cells showing that both human and mouse periostin promoter activity was highly induced by p65, a NFκB subunit (B), and to a lesser extent by other pro-inflammatory transcription factors like c-Jun, STAT1, STAT6 (C), or pro-fibrotic transcription factors like Smad3, Smad4 and Smad5 (D). (E) Endogenous periostin mRNA expression in HEK293 cells was induced after transfection with the indicated transcription factors to a level comparable to the luciferase-assay results. (F to I) ChIP analysis performed in the model of NTS-induced glomerulonephritis, showing high enrichment of the pro-inflammatory transcription factors p65 (F), p-c-Jun (G) and p-STAT1 (H) on several positions of periostin promoter *in vivo* after NTS. On the contrary, p-Smad3, a pro-fibrotic transcription factor, was not enriched on periostin promoter after NTS (I). **P*<0.05, ***P*<0.01 vs. Ct or WT PBS. For mice, *n*=4 per group. For cell cultures, quantifications of three independent experiments performed in triplicates are shown.

Figure 2. Periostin KO mice are protected from the development of NTS-induced glomerulonephritis. (A, B) Periostin mRNA (A) and protein (B) are increased in NTS-induced glomerulonephritis. (C, D) Periostin KO mice are highly protected from the increase in weight (C) and proteinuria (D) caused by NTS. (E) Masson's Trichrome staining showing reduced fibrosis and tissue damage in periostin KO mice. Quantification of glomerular lesions is shown in (F). (G to I) mRNA expression of the fibrotic molecules COL1 (G), COL3 (H) and TGF-β1 (I) is highly decreased in

periostin KO mice after NTS. (J to L) mRNA expression of the inflammatory mediators MCP-1 (J), RANTES (K) and VCAM-1 (L) is diminished in periostin KO mice after NTS. (M, N) F4/80 (M) and CD3 (N) staining showing markedly decreased accumulation of macrophages and lymphocytes, respectively, in periostin KO mice after NTS. Quantification of the staining is shown in the graphs below. mRNA and protein results from the whole kidney are shown (A, B, G-L). Animals were sacrificed after 14 days of NTS administration. **P*<0.05, ***P*<0.01 vs. WT PBS or WT NTS, $^{\#}$*P*<0.05 vs. WT NTS. Scale bars=100 μm (E, M, N). *n*=6-7 per group.

Figure 3. Delayed treatment with antisense against periostin reverses the development of NTS-induced glomerulonephritis. (A**,** B) Periostin mRNA (A) and protein (B) is increased in NTS scrambled-treated mice but is decreased in mice treated with antisense ODN. (C to E) Initiation of antisense treatment at D3 after NTS reversed the increase in weight (C), proteinuria (D) and BUN (E) observed in NTS scrambled-treated mice. (F) Masson's Trichrome staining showing reduced fibrosis and tissue damage in NTS antisense-treated mice. (G, H) Quantification of structural glomerular (G) and tubular (H) alterations showing highly reduced crescent formation, fibrin deposition, glomeruloscrlerosis and tubular dilation in NTS antisense -treated mice. (I to K) mRNA expression of the fibrotic molecules COL1 (I), COL3 (J) and TGF-β1 (K) is attenuated in antisense-treated mice after NTS. (L to N) mRNA expression of the inflammatory mediators MCP-1 (L), VCAM-1 (M) and CSF-1 (N) is diminished in antisense-treated mice after NTS. (O, P) F4/80 (O) and CD3 (P) staining showing markedly decreased accumulation of macrophages and lymphocytes, respectively, in NTS-mice treated with antisense against periostin. Quantification of the staining is shown in the graphs on the right. Animals were

sacrificed after 9 days of NTS administration. *P<0.05, **P<0.01 vs. PBS, $^{\#}P$<0.05 $^{\#\#}P$<0.01 vs. NTS scrambled. Scale bars=100 μm (F, O, P). n=5 per group.

Figure 4. Periostin and integrin-β3 are co-localized at the sites of injury in the model of NTS-induced glomerulonephritis. (A, D) Immunohistochemical staining for periostin in WT/KO (A) and scrambled/antisense (D) mice showing increased expression of periostin in glomeruli and vessels of WT NTS mice that is absent in KO and ameliorated in antisense mice. (B, E) Integrin-β3 mRNA expression is induced in WT NTS (B) and NTS scrambled (E) mice but is highly ameliorated in KO NTS and NTS antisense mice, respectively. (C, F) Immunohistochemical localization of integrin-β3 in WT/KO (C) and scrambled/antisense (F) mice showing increased expression in glomeruli and vessels of WT NTS mice that is highly attenuated in KO and antisense mice, respectively. (G) Immunohistochemical staining of integrin-β3 and periostin in serial sections of WT NTS mice, showing localization of both proteins at the same sites. (H) Double immunofluorescence for periostin (green)/nestin (red) and integrin-β3 (green)/nestin (red) in WT NTS mice, showing that both periostin and integrin-β3 are expressed by podocytes in glomeruli of NTS mice. (I) Double immunofluorescence for periostin or integrin-β3 (green) with CD44 (red) in WT NTS mice showed that both proteins are strongly expressed by activated parietal epithelial cells. Double immunofluorescence for periostin (green) with α-SMA or CD146 (red) showed no co-localization with mesangial and endothelial cells, respectively. (J) Co-IP analysis using anti-integrin-β3 antibody successfully precipitated both integrin-β3 and periostin showing that the two proteins interact *in vivo* in the NTS model. The samples were run on the same gel but were discontinuous. Animals were sacrificed after 14 or 9 days of NTS in the series of

experiments with the KO (A-C) or the antisense (D-J), respectively. *P<0.05 vs. WT PBS, $^{\#}P$<0.05 vs. WT NTS or NTS scrambled. Scale bars=100 μm (G) or 50 μm (A, C, D, F, H). Representative images are shown. n=5-7 per group.

Figure 5. Periostin promotes integrin-β3 signaling *in vivo* and *in vitro*. (A) pFAK expression in WT/KO NTS mice is shown by Western blot. The increase in FAK phosphorylation observed in WT mice after NTS is blunted in KO mice. (B) Immunohistochemical staining of pAKT shows up-regulation in glomeruli and vessels in WT mice after NTS, which is blunted in KO mice. (C) Double immunofluorescence for p-FAK and p-AKT (green) with CD44 or nestin (red) showed that both proteins are expressed by activated parietal epithelial cells and podocytes in the glomeruli of NTS mice. (D) E11 immortalized podocytes were incubated with recombinant mouse periostin (400ng/ml) for the indicated time points and western blot analysis was performed for integrin-β3, pFAK, pAKT and GAPDH, with quantification graphs shown on the right. At 6 hours of periostin incubation integrin-β3 and its downsteam effectors pFAK and pAKT were up-regulated. (E) E11 cells were incubated for 6 hours with increasing doses of recombinant mouse periostin (400 and 1000 ng/ml), followed by western blot analysis of integrin-β3, pFAK, FAK, pAKT, AKT and GAPDH. Quantifications are shown on the right. pFAK and pAKT remain elevated after incubation with increasing doses of periostin. *P<0.05 vs. Ct, **P<0.01 vs. WT PBS or Ct. Scale bars=100 μm (B, C). For mice, n=6-7 per group. Animals were sacrificed after 14 days of NTS administration. For cell cultures, quantifications of three independent experiments performed in triplicates are shown.

Figure 6. Periostin and integrin-β3 are co-expressed in human renal biopsies. (A) Immunohistochemical staining of integrin-β3 and periostin in consecutive sections from an ANCA Vasculitis patient biopsy, depicting a strong expression and a high degree of co-localization between periostin and integrin-β3 both in damaged glomeruli and tubules. (B) Magnified images of the panels drawn in (A), showing in more detail the co-expression of periostin and integrin-β3 in damaged glomeruli and surrounding tubules. Arrows indicate co-localization sites. Scale bars=100 μm (A) or 30 μm (B). Representative images are shown.

Figure 7. Proposed mechanism of how periostin mediates renal damage. Pro-inflammatory transcription factors, with major being NFκB, induce expression of periostin which in turn activates integrin-β3 inducing integrin downstream signaling and leading to cell motility, survival and podocyte foot process effacement. In parallel, periostin promotes the tissue expression of several chemokines (MCP-1, RANTES, VCAM-1, CSF-1) and pro-fibrotic molecules (COL1, COL3, TGF-β1) inducing inflammatory cell infiltration and matrix stabilization, while podocyte damage further amplifies these effects causing a vicious circle.

Figure 1

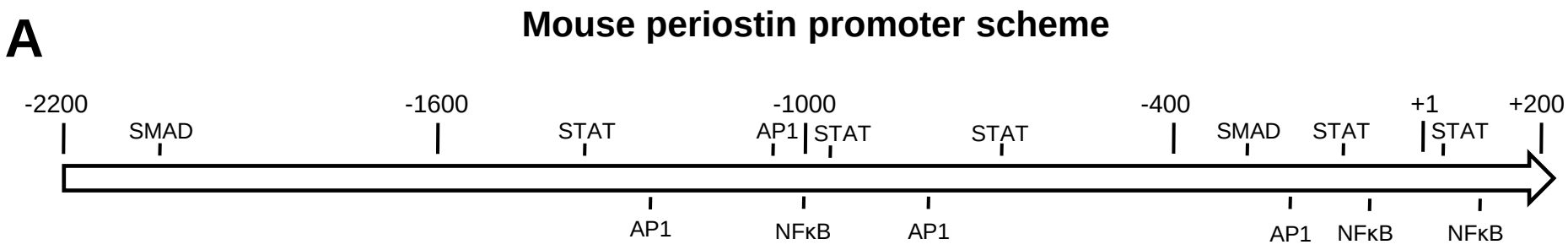
A
Mouse periostin promoter scheme
-2200
-1600
-1000
-400
+1
+200
SMAD
STAT
AP1
STAT
STAT
SMAD
STAT
STAT
AP1
NFκB
AP1
AP1
NFκB
NFκB

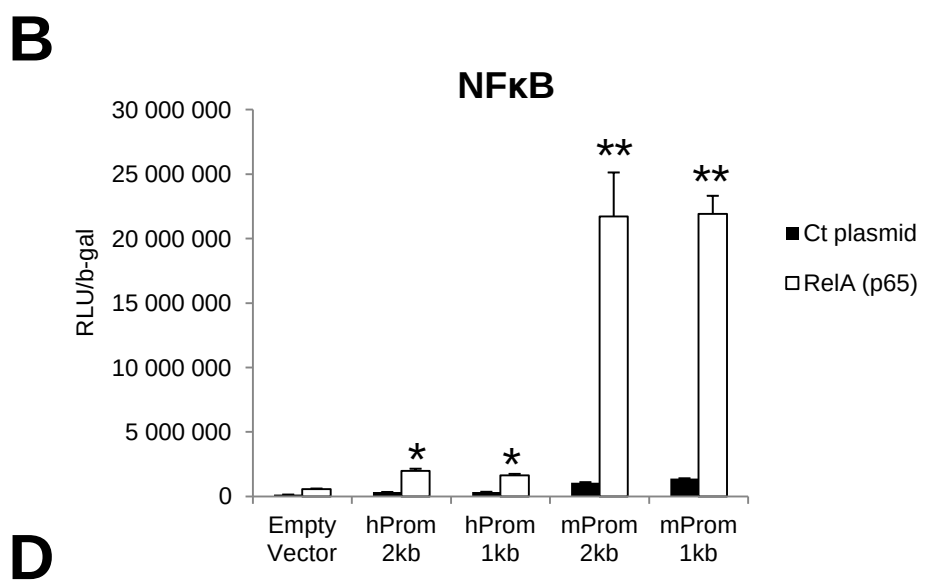
B
NFκB
RLU/b-gal
30 000 000
25 000 000
20 000 000
15 000 000
10 000 000
5 000 000
0
Empty Vector
hProm 2kb
hProm 1kb
mProm 2kb
mProm 1kb
Ct plasmid
RelA (p65)

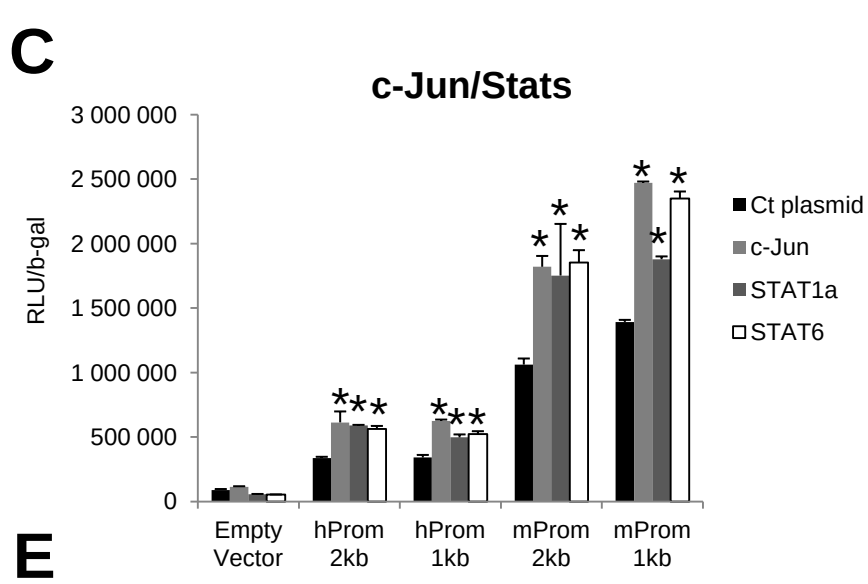
C
c-Jun/Stats
RLU/b-gal
3 000 000
2 500 000
2 000 000
1 500 000
1 000 000
500 000
0
Empty Vector
hProm 2kb
hProm 1kb
mProm 2kb
mProm 1kb
Ct plasmid
c-Jun
STAT1a
STAT6

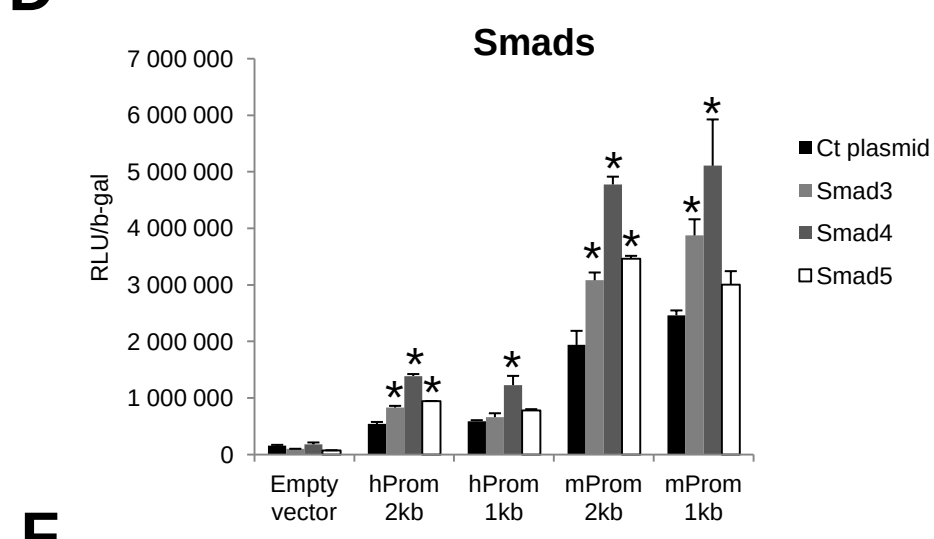
D
Smads
RLU/b-gal
7 000 000
6 000 000
5 000 000
4 000 000
3 000 000
2 000 000
1 000 000
0
Empty vector
hProm 2kb
hProm 1kb
mProm 2kb
mProm 1kb
Ct plasmid
Smad3
Smad4
Smad5

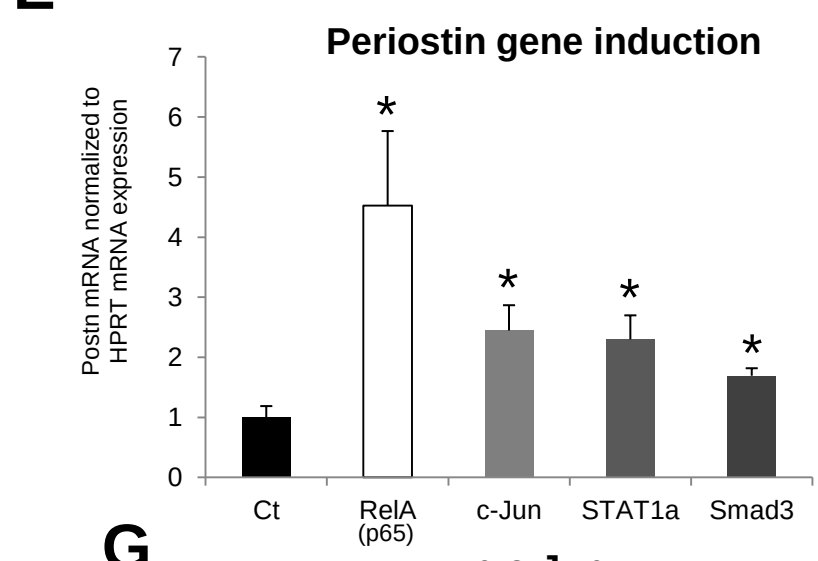
E
Periostin gene induction
Postn mRNA normalized to HPRT mRNA expression
7
6
5
4
3
2
1
0
Ct
RelA (p65)
c-Jun
STAT1a
Smad3

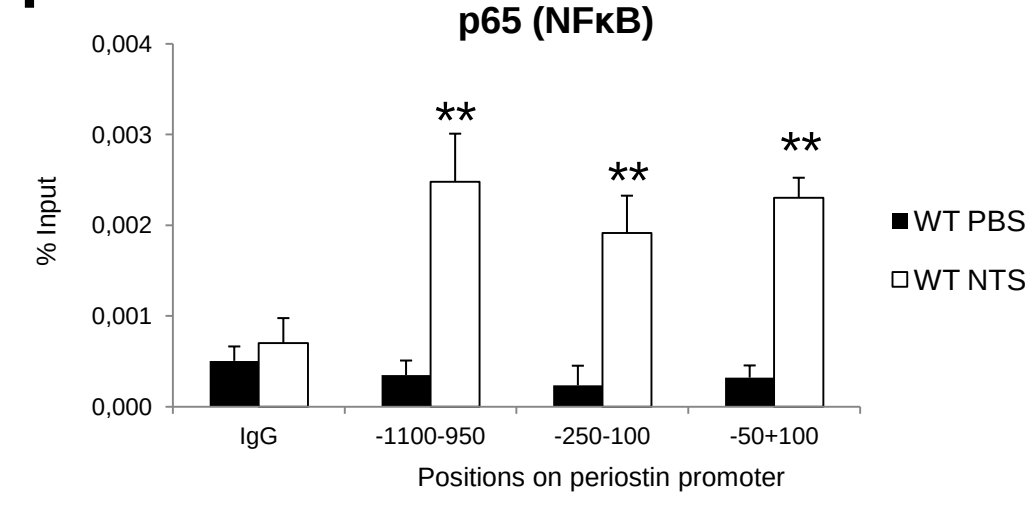
F
p65 (NFκB)
% Input
0,004
0,003
0,002
0,001
0,000
IgG
-1100-950
-250-100
-50+100
Positions on periostin promoter
WT PBS
WT NTS

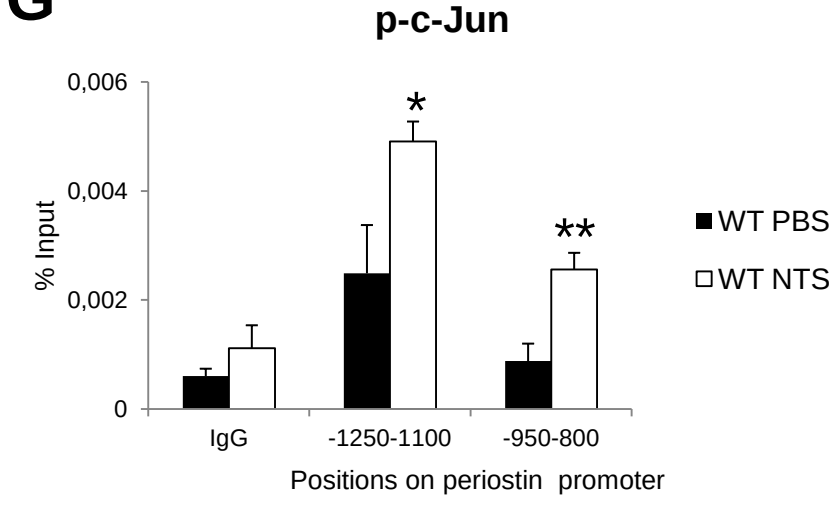
G
p-c-Jun
% Input
0,006
0,004
0,002
0
IgG
-1250-1100
-950-800
Positions on periostin promoter
WT PBS
WT NTS

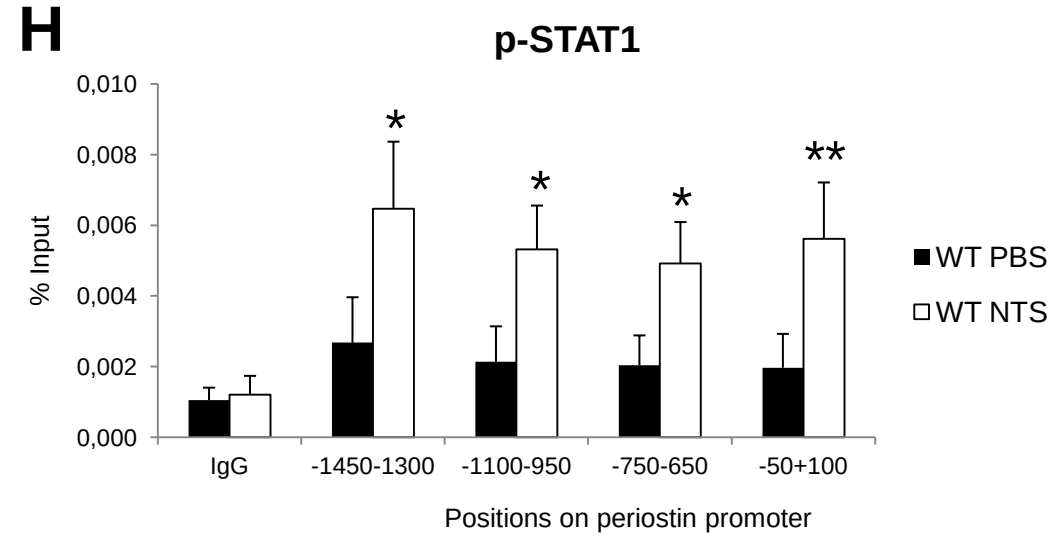
H
p-STAT1
% Input
0,010
0,008
0,006
0,004
0,002
0,000
IgG
-1450-1300
-1100-950
-750-650
-50+100
Positions on periostin promoter
WT PBS
WT NTS

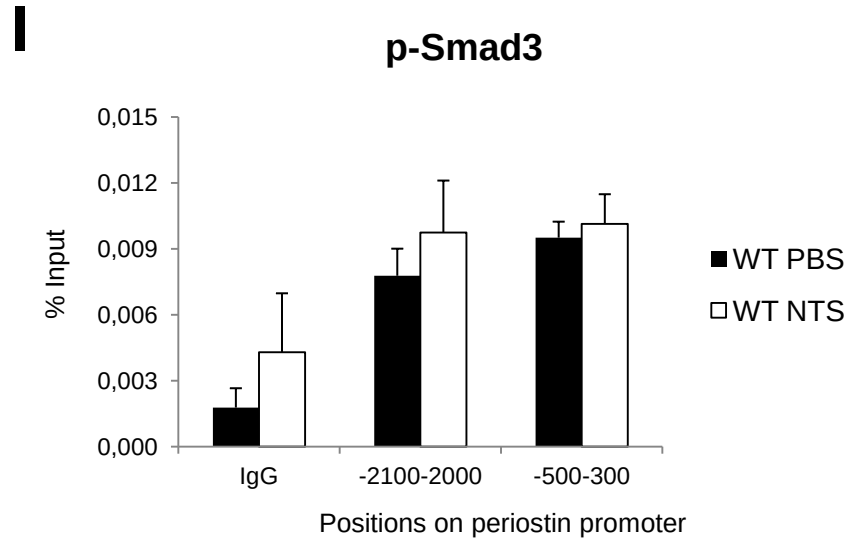
I
p-Smad3
% Input
0,015
0,012
0,009
0,006
0,003
0,000
IgG
-2100-2000
-500-300
Positions on periostin promoter
WT PBS
WT NTS

Figure 2A-F

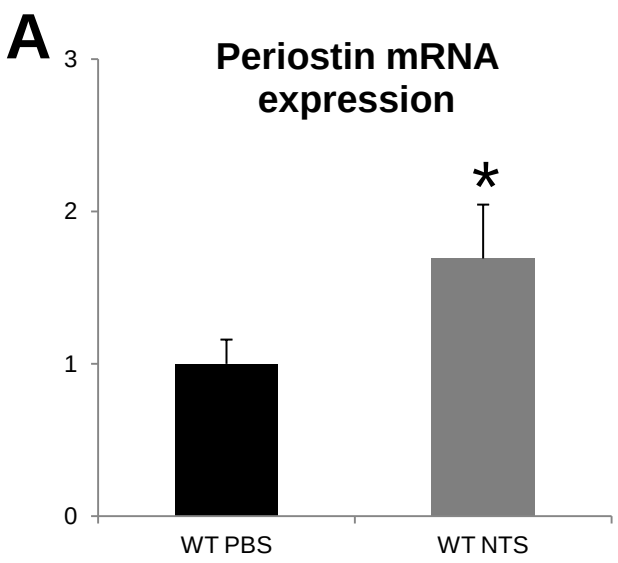
A
Periostin mRNA expression
3
2
1
0
*
WT PBS
WT NTS

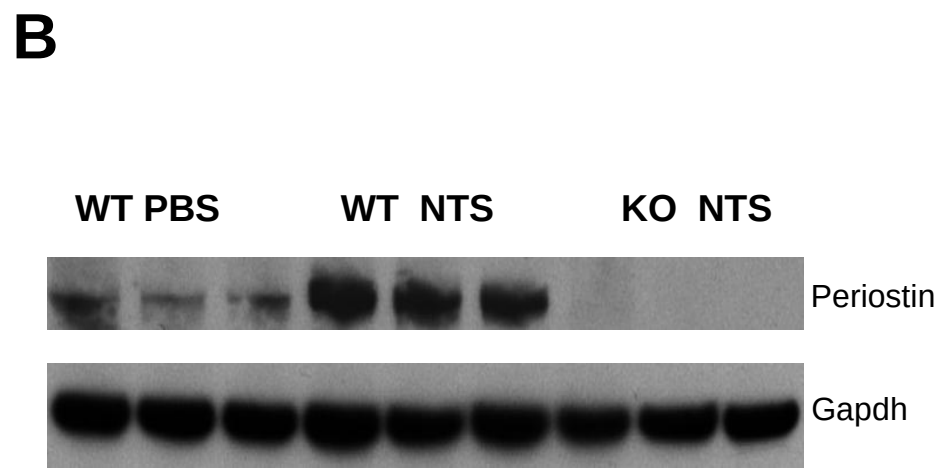
B
WT PBS
WT NTS
KO NTS
Periostin
Gapdh

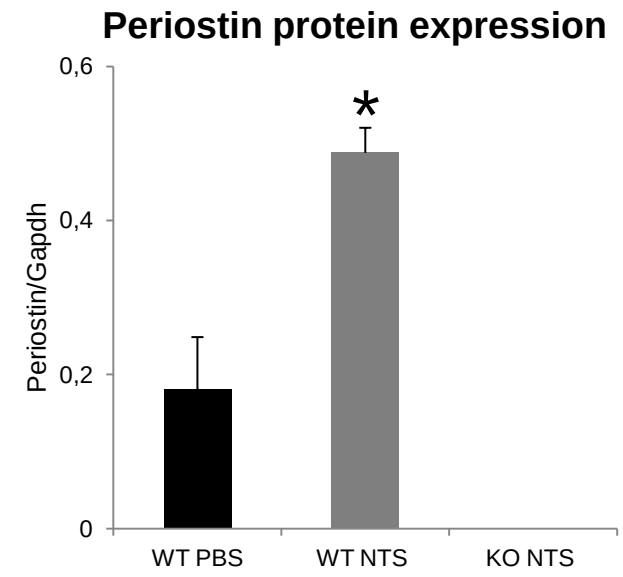
Periostin protein expression
0,6
0,4
0,2
0
Periostin/Gapdh
*
WT PBS
WT NTS
KO NTS

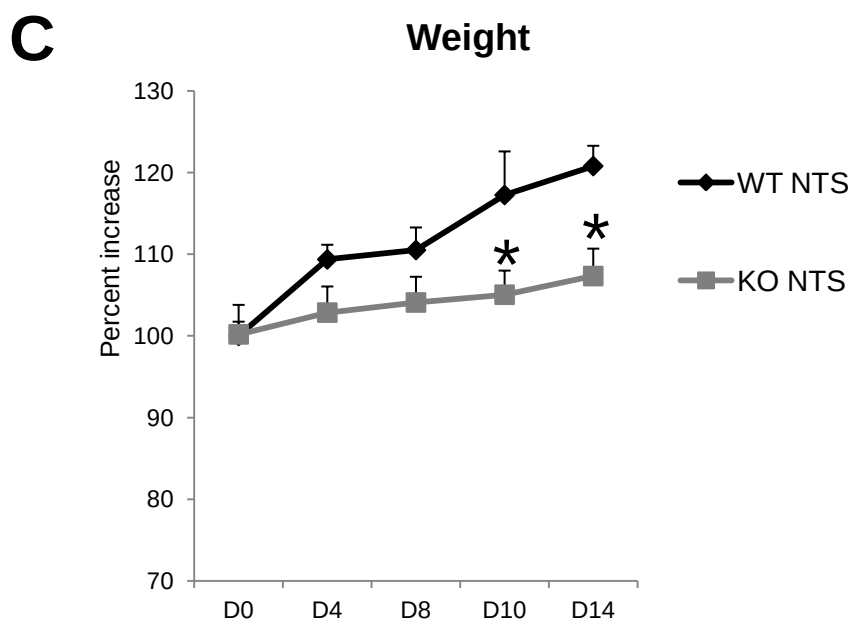
C
Weight
130
120
110
100
90
80
70
Percent increase
WT NTS
KO NTS
*
*
D0
D4
D8
D10
D14

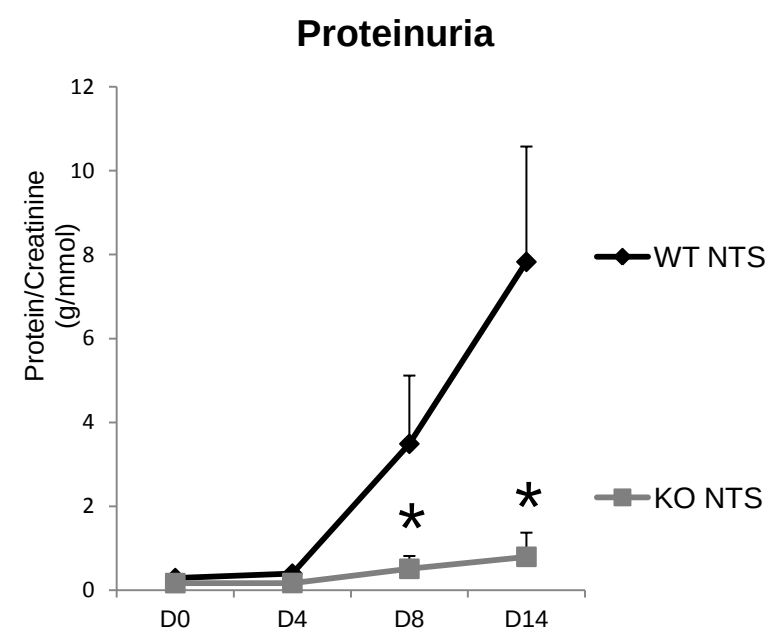
D
Proteinuria
12
10
8
6
4
2
0
Protein/Creatinine (g/mmol)
WT NTS
KO NTS
*
*
D0
D4
D8
D14

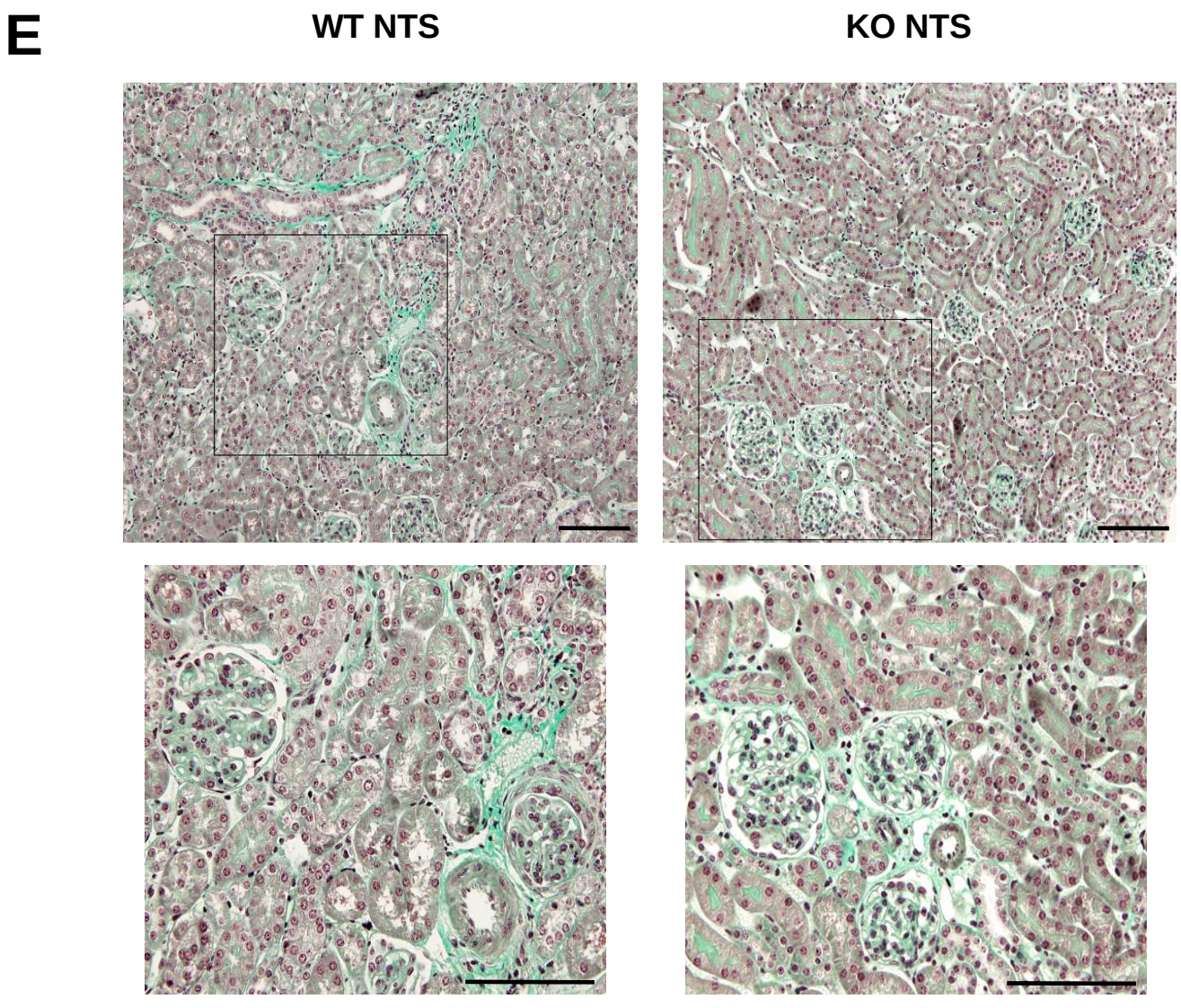
E
WT NTS
KO NTS


F
Glomerular lesions
60
50
40
30
20
10
0
% injured glomeruli
**
WT NTS
KO NTS

Figure 2G-N

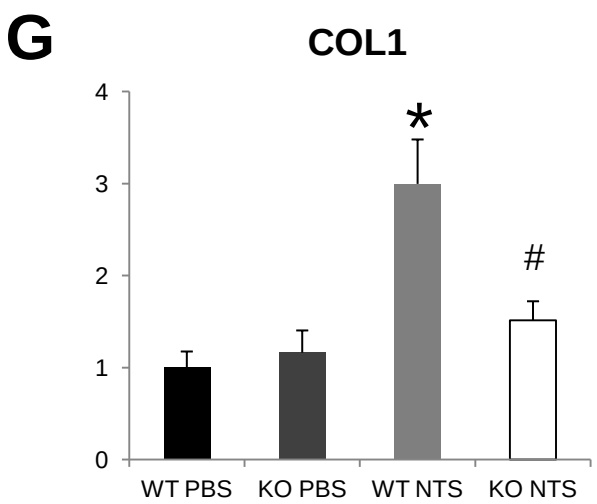
G
COL1
4
3
2
1
0
*
#
WT PBS
KO PBS
WT NTS
KO NTS

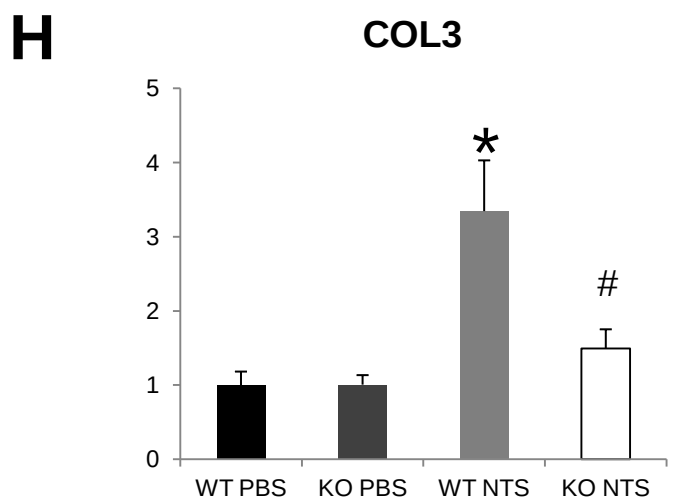
H
COL3
5
4
3
2
1
0
*
#
WT PBS
KO PBS
WT NTS
KO NTS

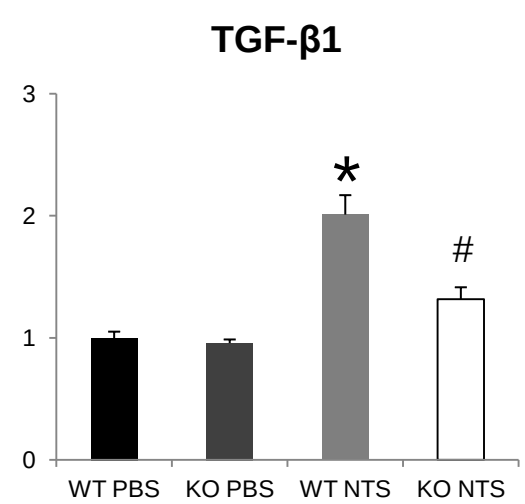
I
TGF-β1
3
2
1
0
*
#
WT PBS
KO PBS
WT NTS
KO NTS

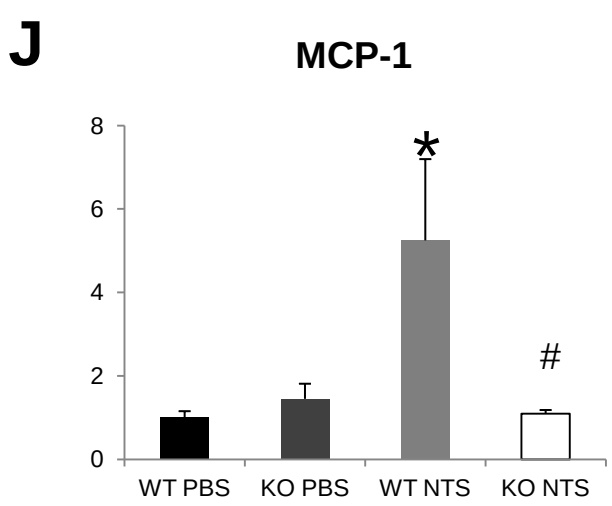
J
MCP-1
8
6
4
2
0
*
#
WT PBS
KO PBS
WT NTS
KO NTS

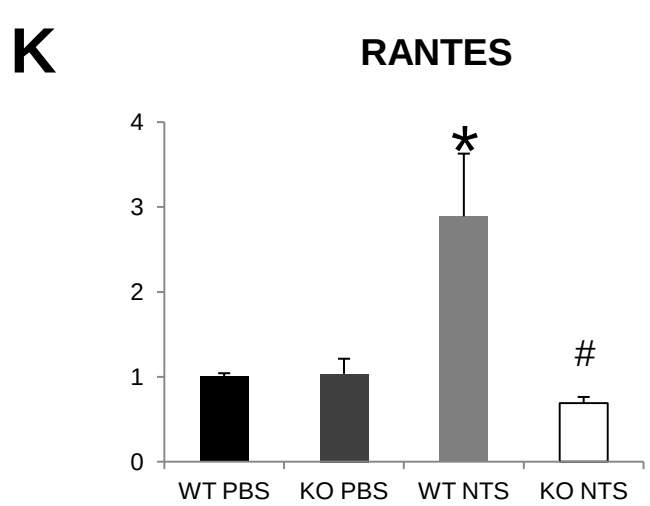
K
RANTES
4
3
2
1
0
*
#
WT PBS
KO PBS
WT NTS
KO NTS

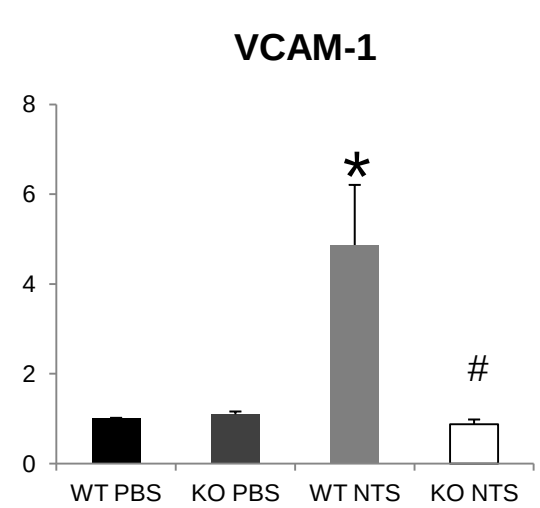
L
VCAM-1
8
6
4
2
0
*
#
WT PBS
KO PBS
WT NTS
KO NTS

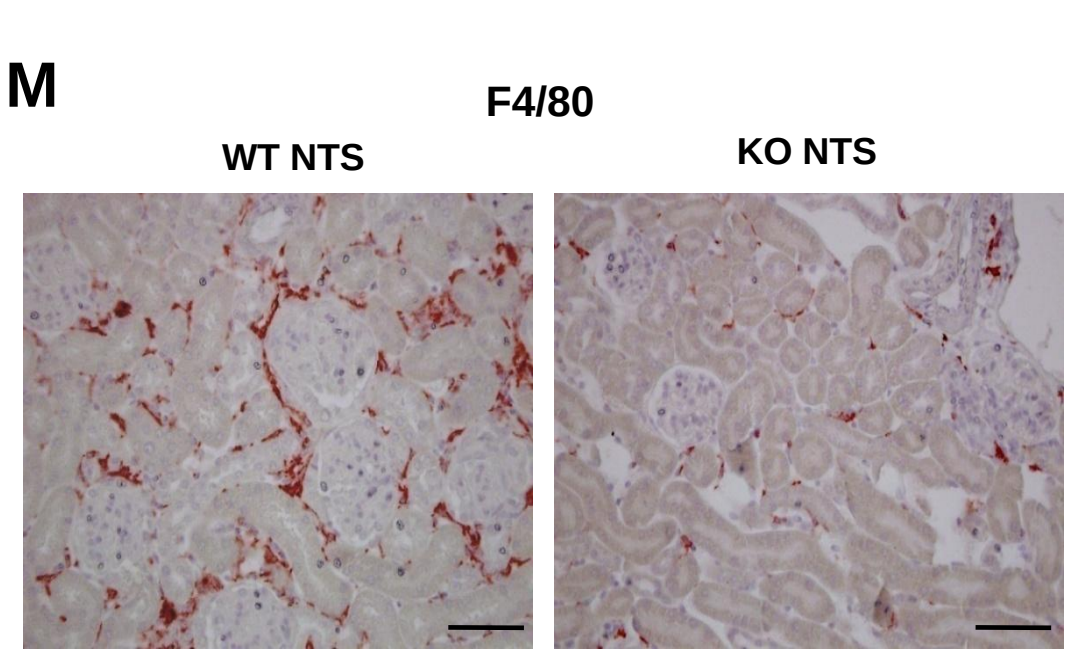
M
F4/80
WT NTS
KO NTS

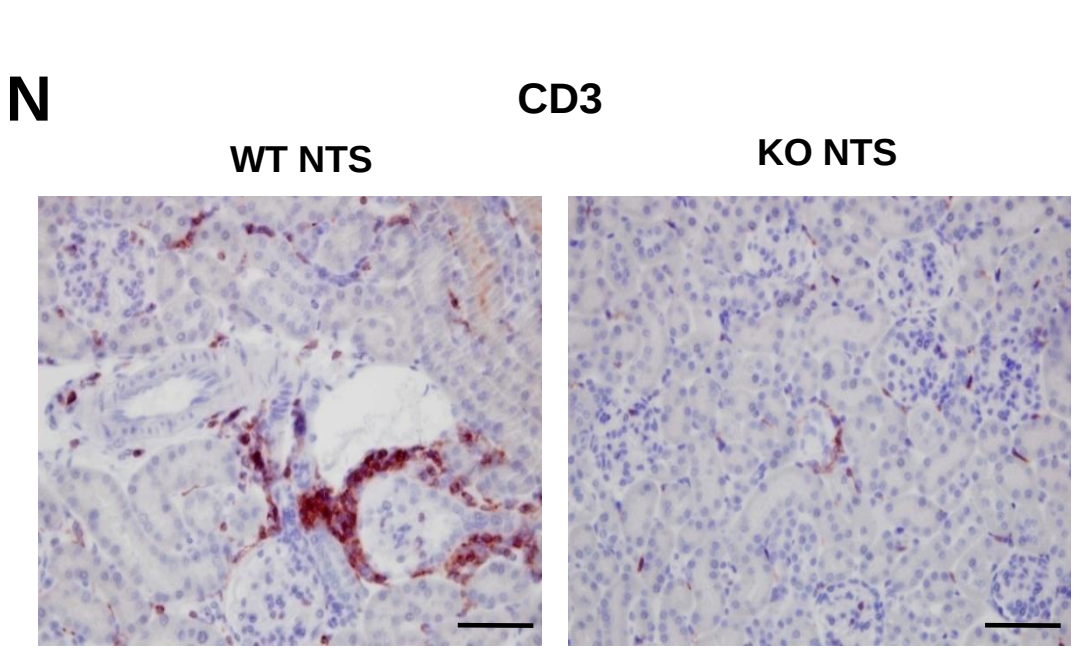
N
CD3
WT NTS
KO NTS

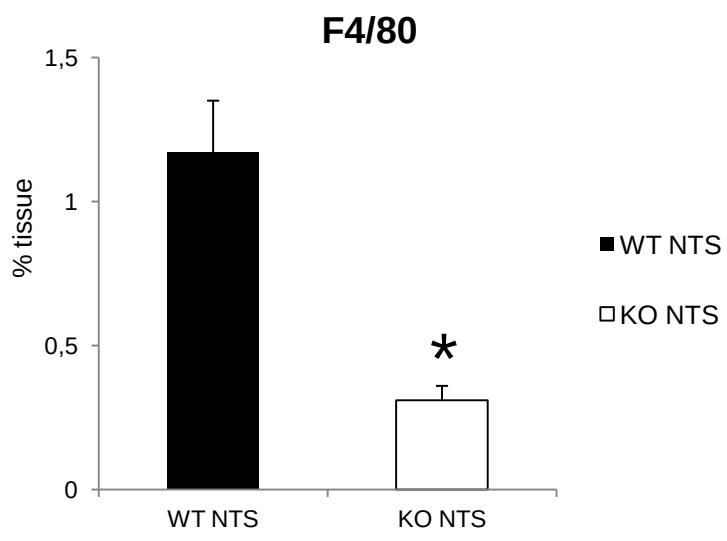
F4/80
1,5
1
0,5
0
% tissue
*
WT NTS
KO NTS
WT NTS
KO NTS

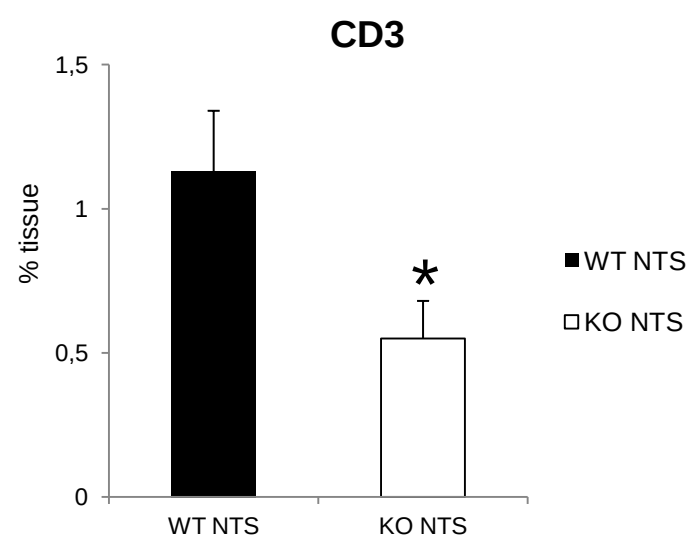
CD3
1,5
1
0,5
0
% tissue
*
WT NTS
KO NTS
WT NTS
KO NTS

Figure 3A-H

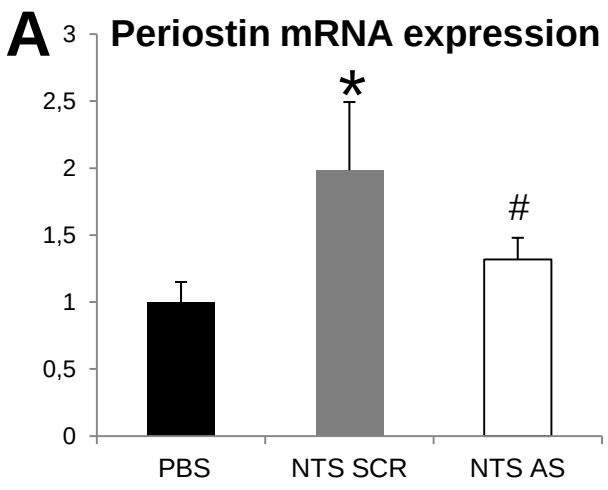
A
Periostin mRNA expression
3
2,5
2
1,5
1
0,5
0
*
#
PBS
NTS SCR
NTS AS

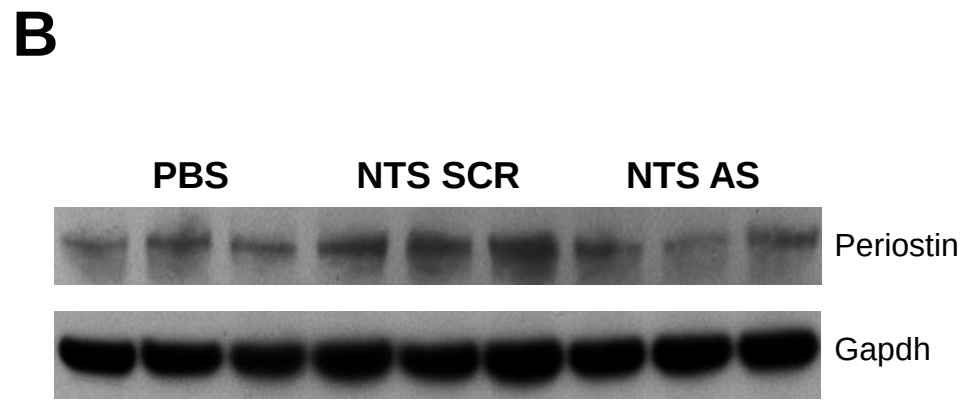
B
PBS
NTS SCR
NTS AS
Periostin
Gapdh

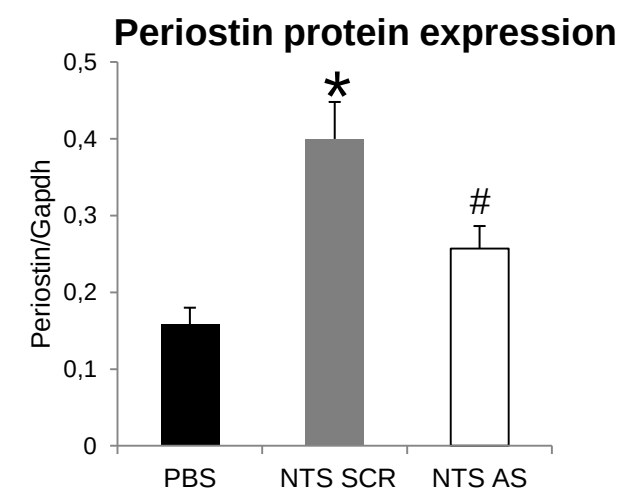
Periostin protein expression
0,5
0,4
0,3
0,2
0,1
0
Periostin/Gapdh
*
#
PBS
NTS SCR
NTS AS

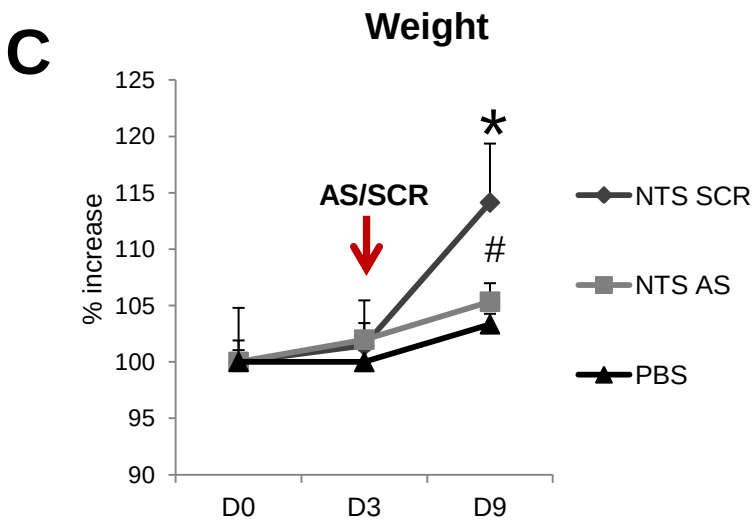
C
Weight
125
120
115
110
105
100
95
90
% increase
AS/SCR
*
#
NTS SCR
NTS AS
PBS
D0
D3
D9

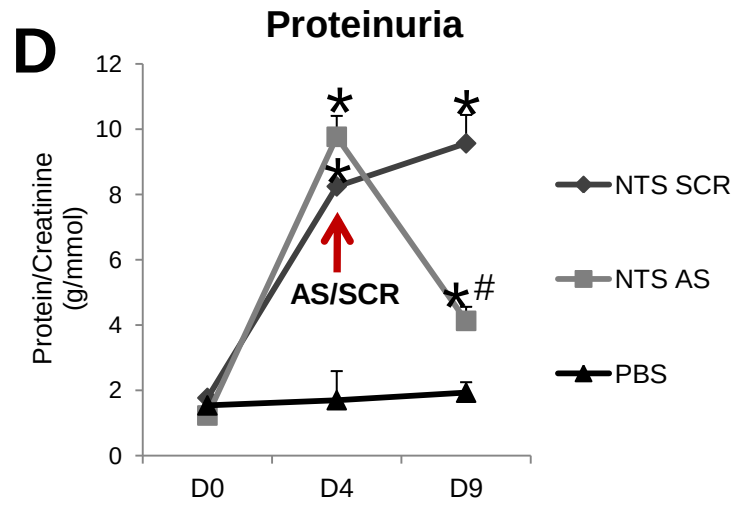
D
Proteinuria
12
10
8
6
4
2
0
Protein/Creatinine (g/mmol)
*
*
*
*#
AS/SCR
NTS SCR
NTS AS
PBS
D0
D4
D9

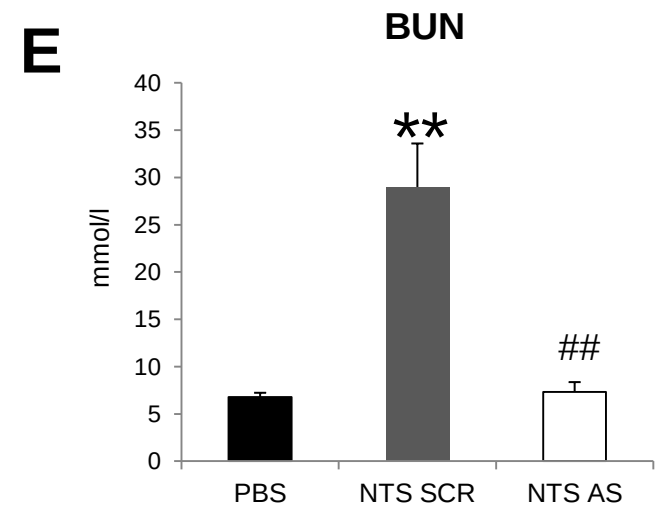
E
BUN
40
35
30
25
20
15
10
5
0
mmol/l
**
##
PBS
NTS SCR
NTS AS

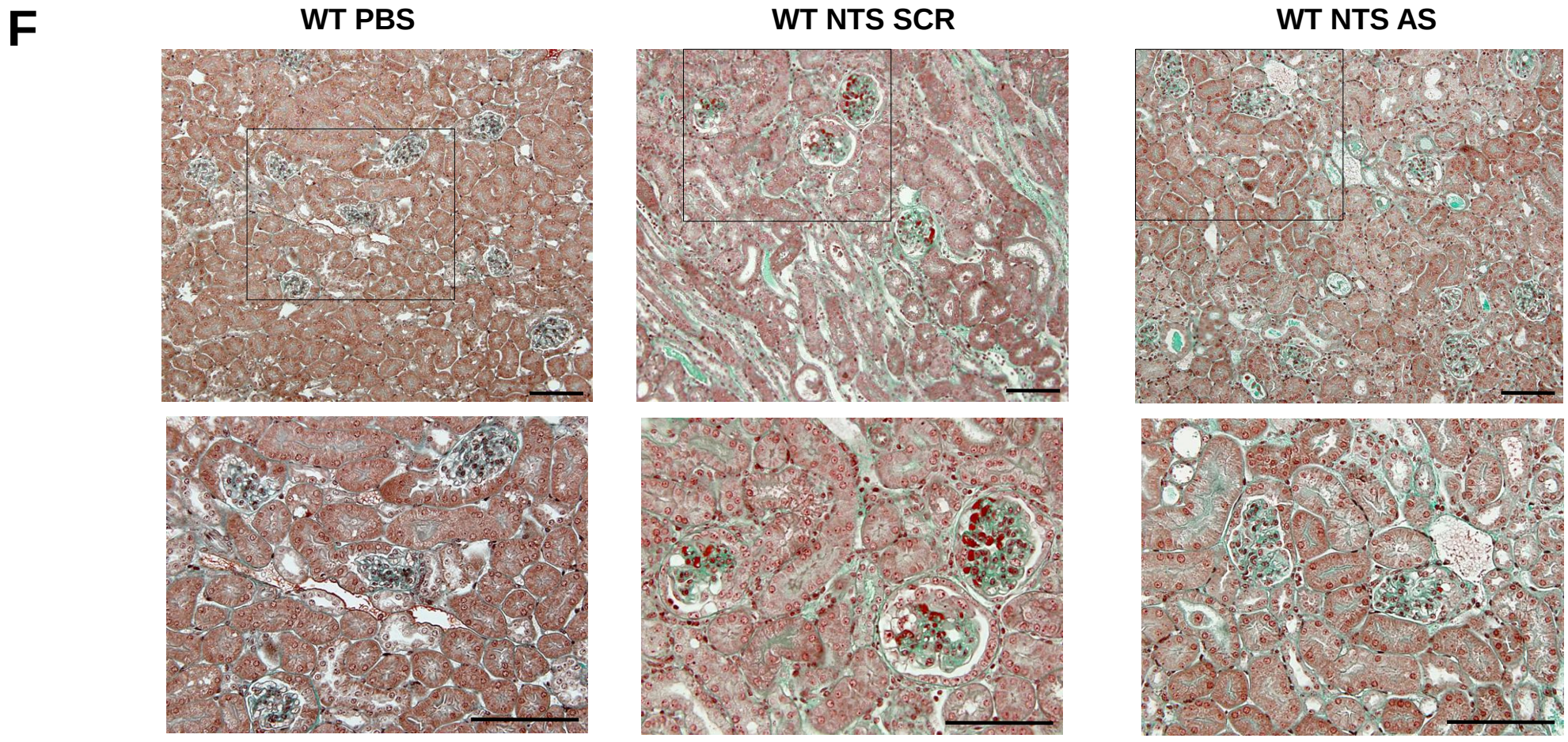
F
WT PBS
WT NTS SCR
WT NTS AS

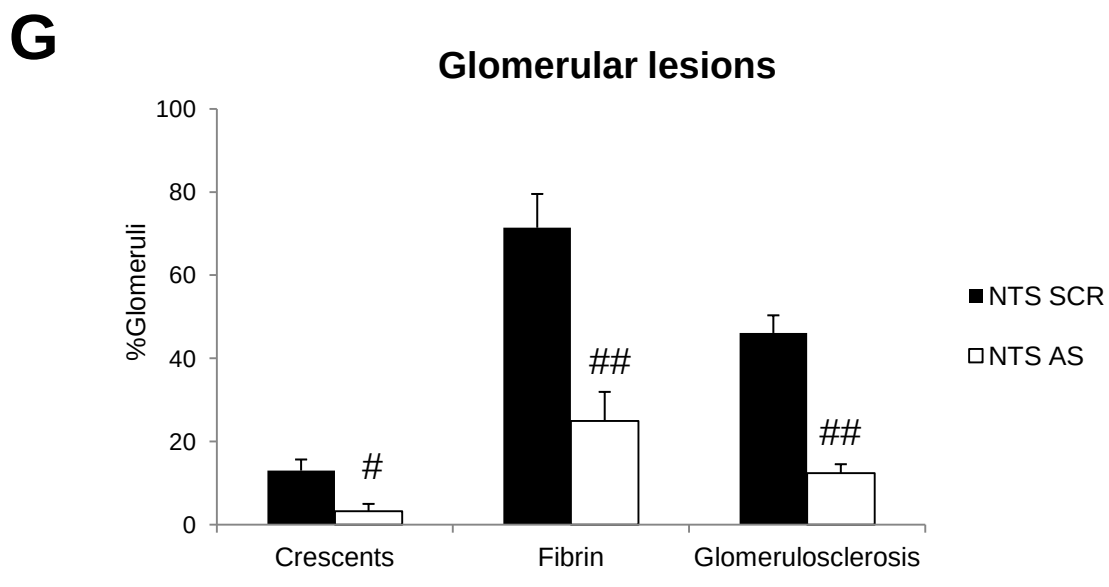
G
Glomerular lesions
100
80
60
40
20
0
%Glomeruli
#
##
##
NTS SCR
NTS AS
Crescents
Fibrin
Glomerulosclerosis

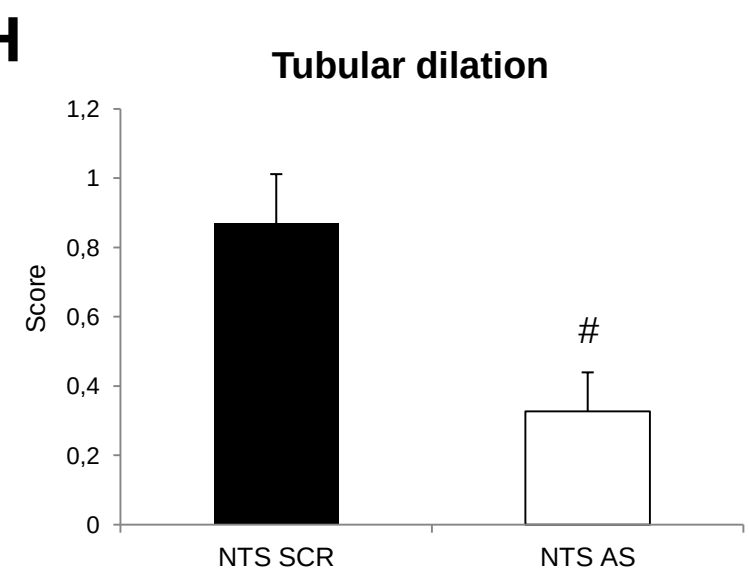
H
Tubular dilation
1,2
1
0,8
0,6
0,4
0,2
0
Score
#
NTS SCR
NTS AS

Figure 3I-P

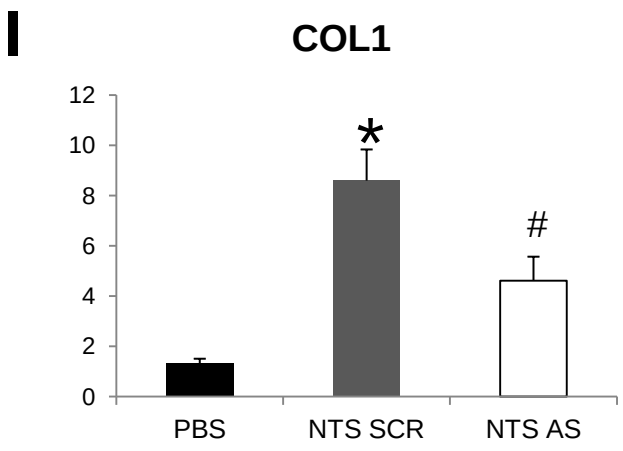
I
COL1
12
10
8
6
4
2
0
*
#
PBS
NTS SCR
NTS AS

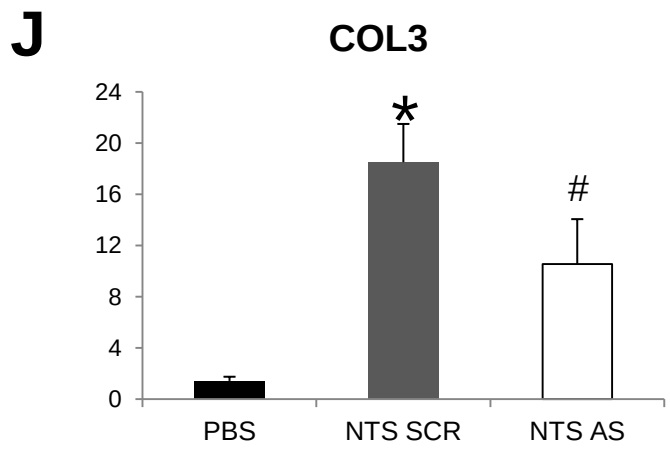
J
COL3
24
20
16
12
8
4
0
*
#
PBS
NTS SCR
NTS AS

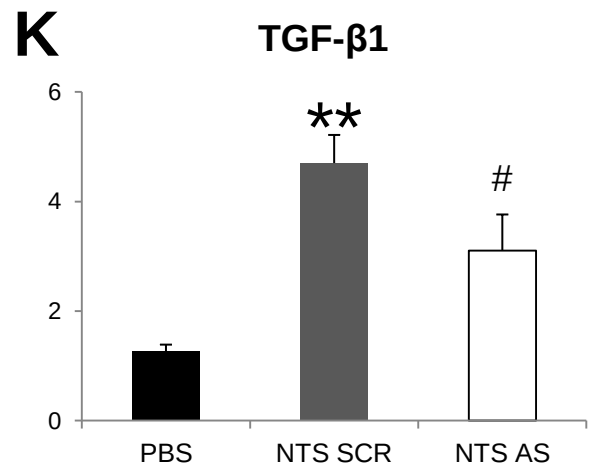
K
TGF-β1
6
4
2
0
**
#
PBS
NTS SCR
NTS AS

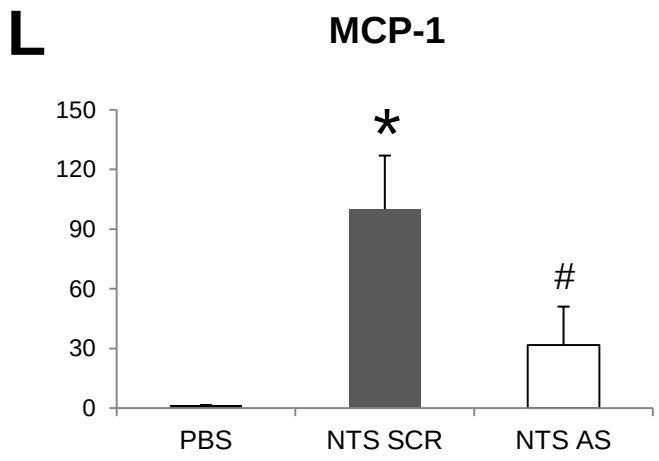
L
MCP-1
150
120
90
60
30
0
*
#
PBS
NTS SCR
NTS AS

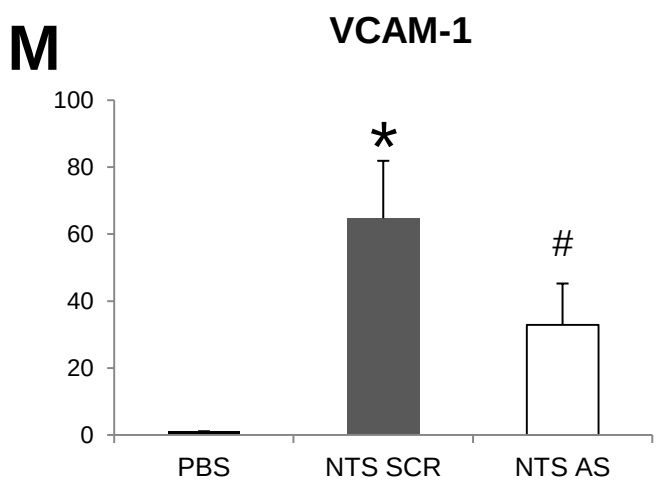
M
VCAM-1
100
80
60
40
20
0
*
#
PBS
NTS SCR
NTS AS

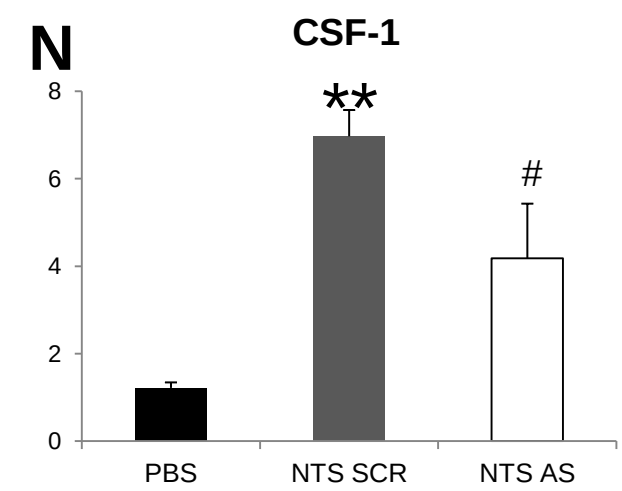
N
CSF-1
8
6
4
2
0
**
#
PBS
NTS SCR
NTS AS

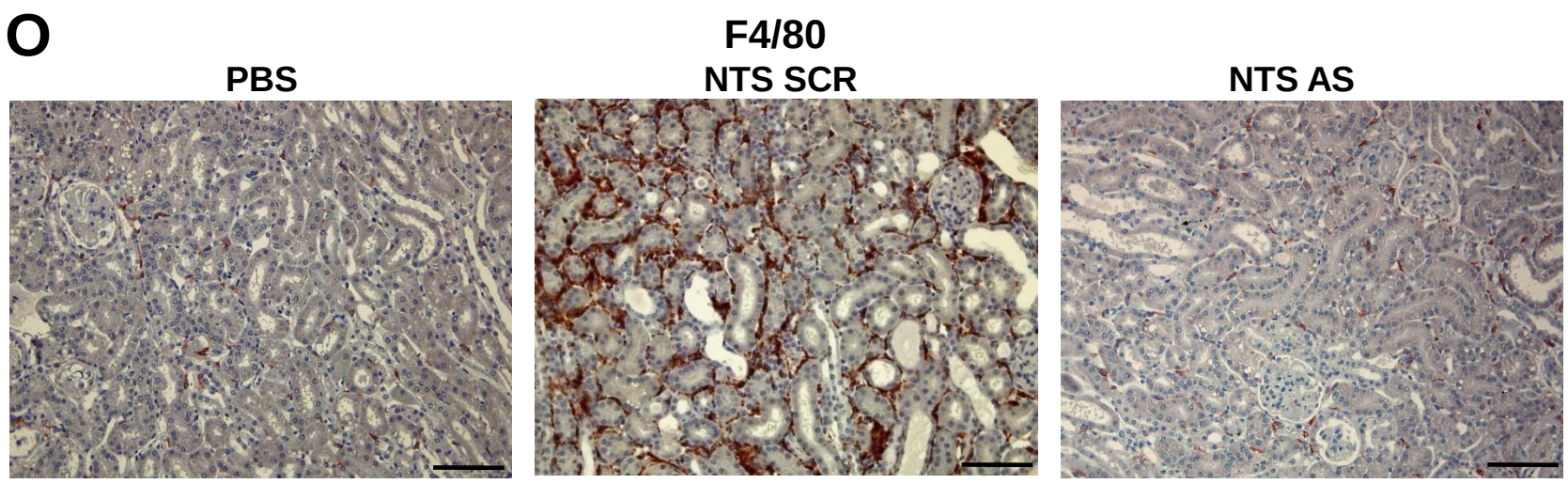
O
F4/80
PBS
NTS SCR
NTS AS

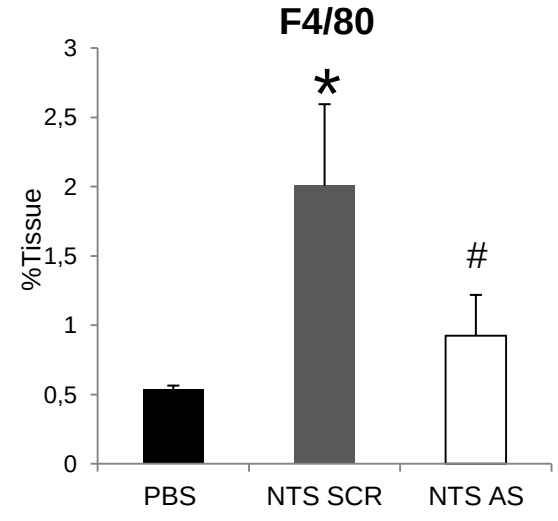
F4/80
%Tissue
3
2,5
2
1,5
1
0,5
0
*
#
PBS
NTS SCR
NTS AS

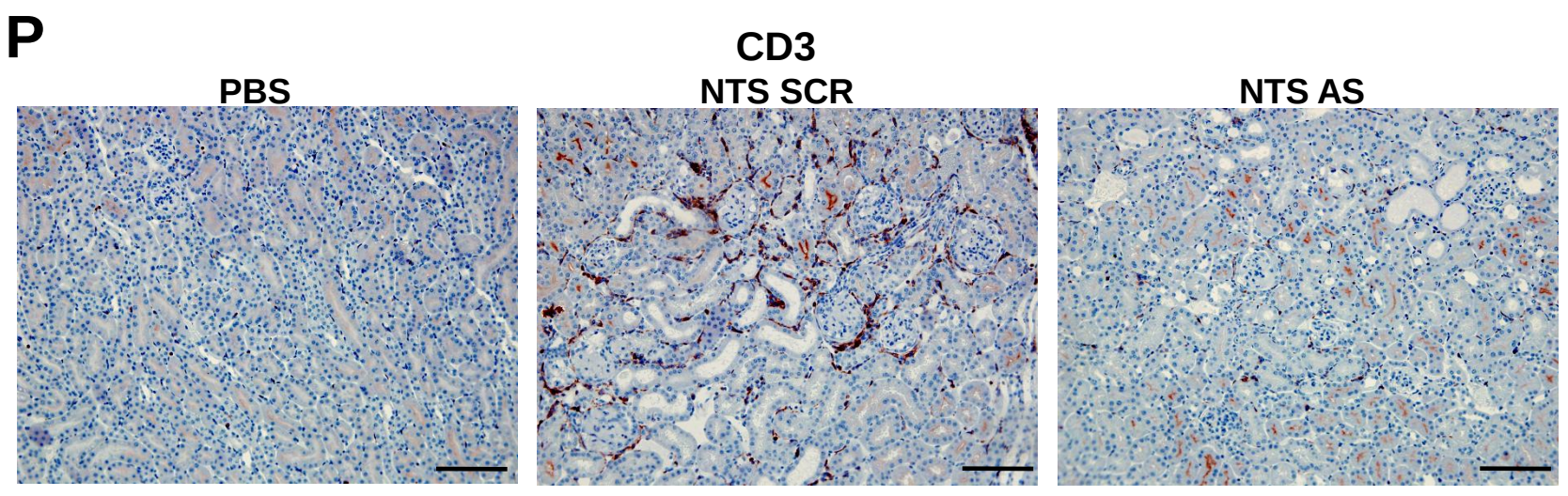
P
CD3
PBS
NTS SCR
NTS AS

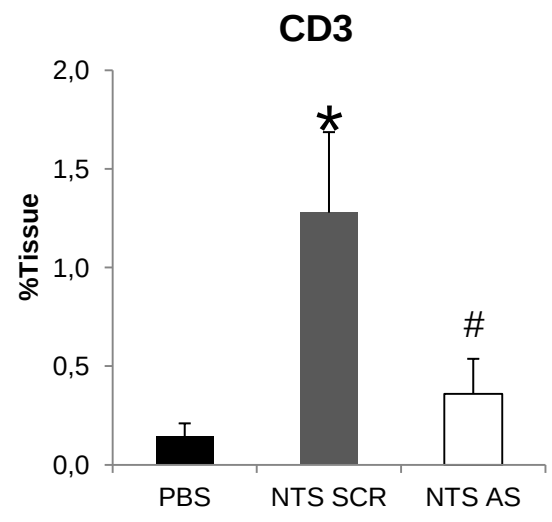
CD3
%Tissue
2,0
1,5
1,0
0,5
0,0
*
#
PBS
NTS SCR
NTS AS

Figure 4A-F

A

PERIOSTIN

WT PBS | **WT NTS** | **KO NTS**

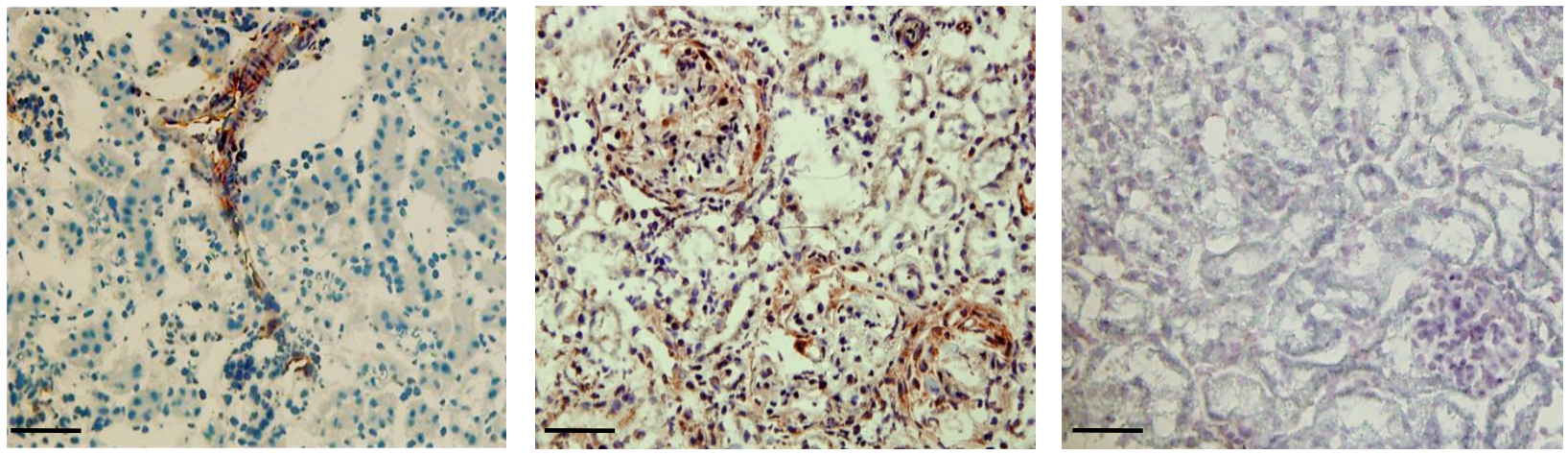

B

ITGβ3 mRNA

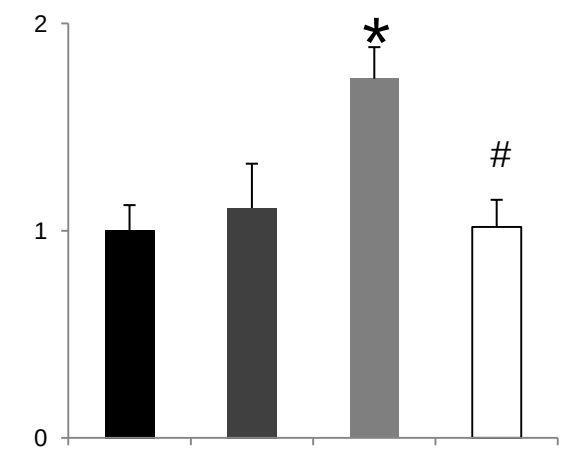

C

ITGB3

WT PBS | **WT NTS** | **KO NTS**

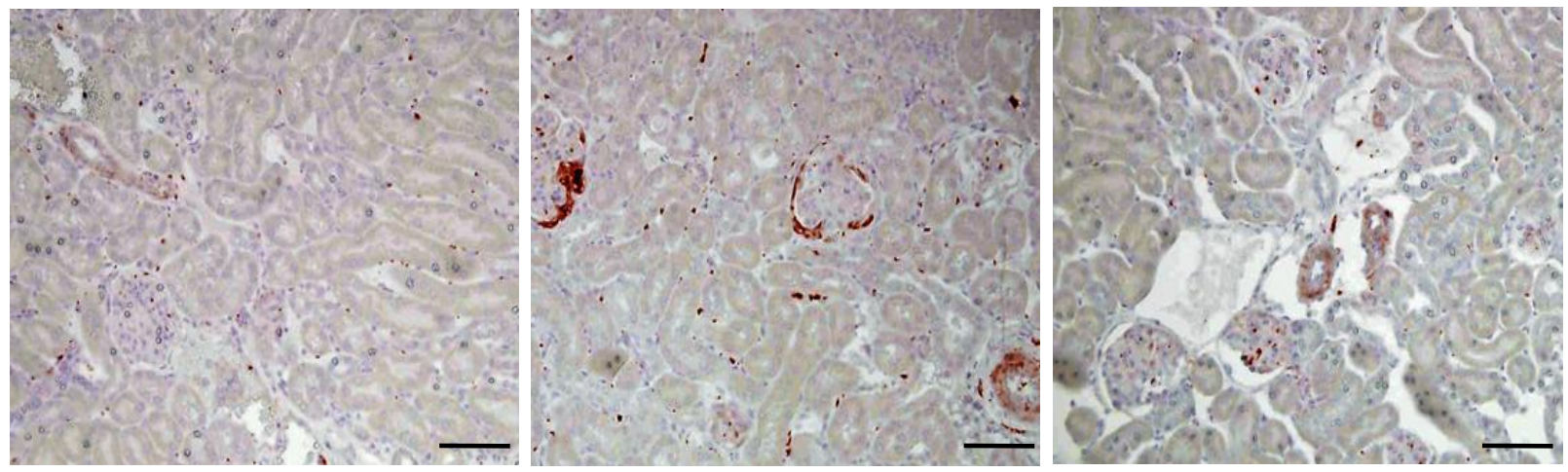

D

PERIOSTIN

PBS | **NTS SCR** | **NTS AS**

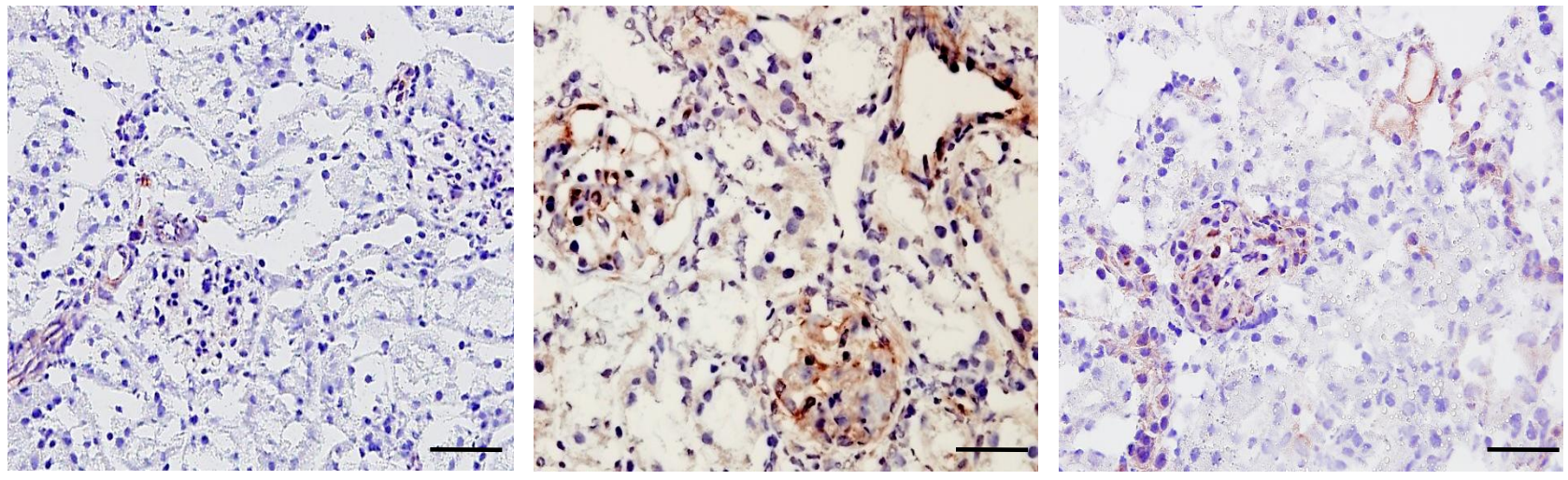

E

ITGβ3 mRNA

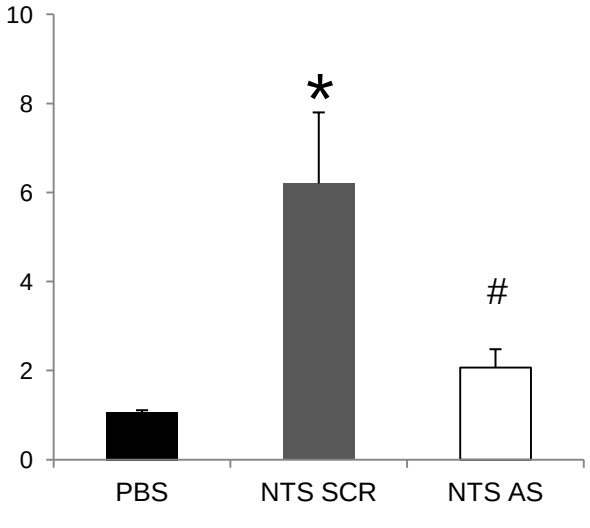

F

ITGB3

PBS | **NTS SCR** | **NTS AS**

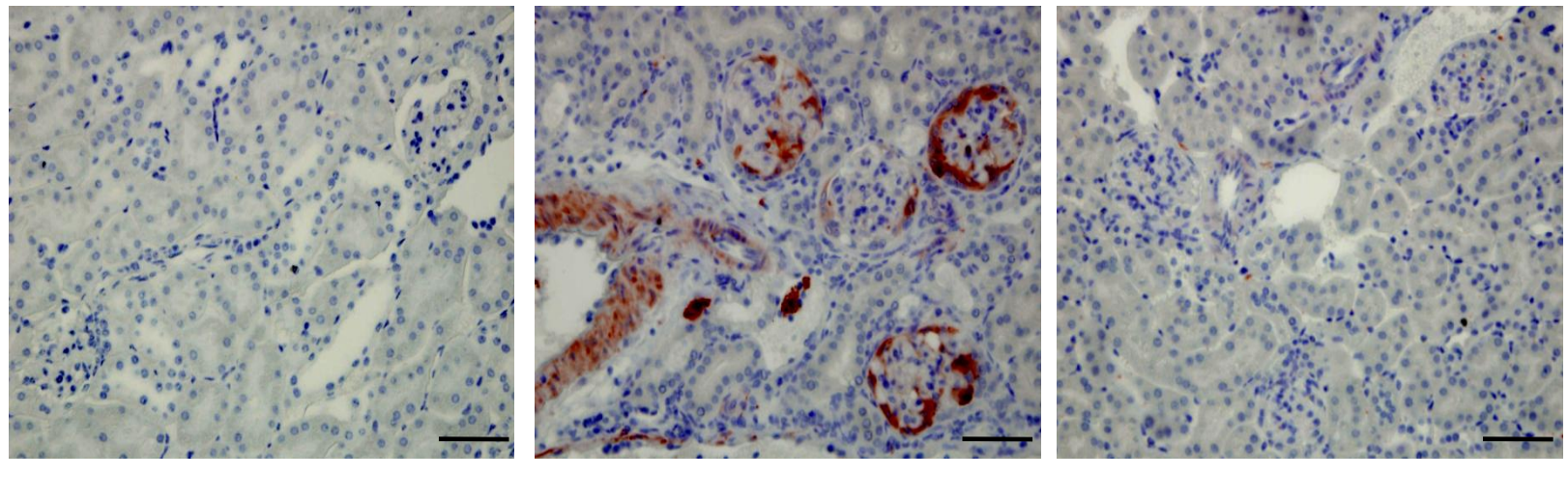

Figure 4G-J

G

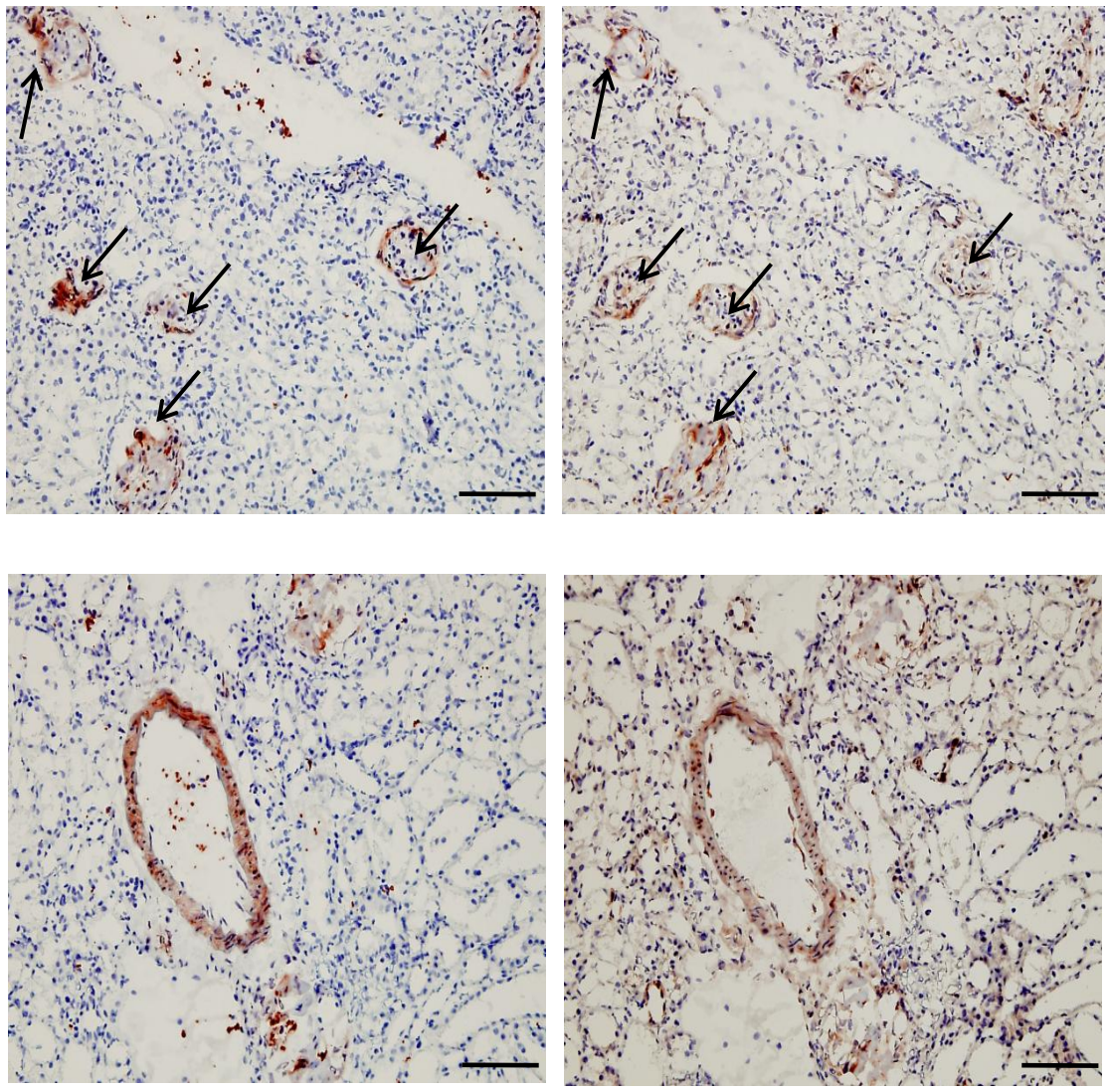

H

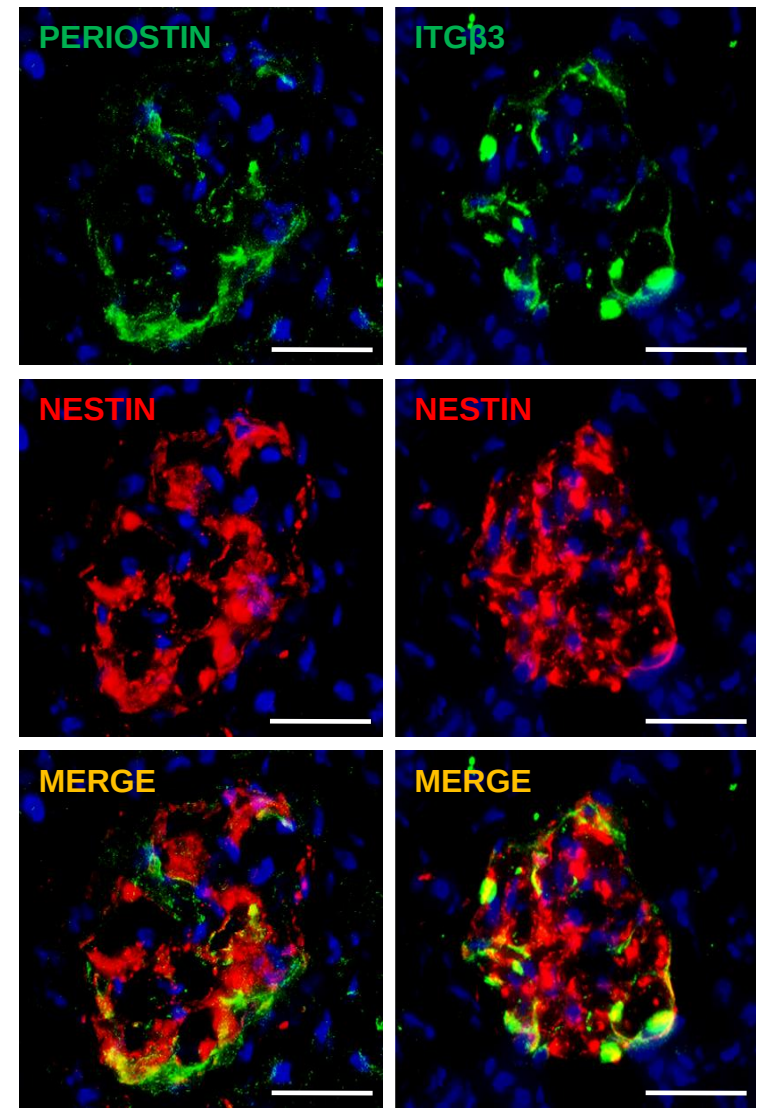

I

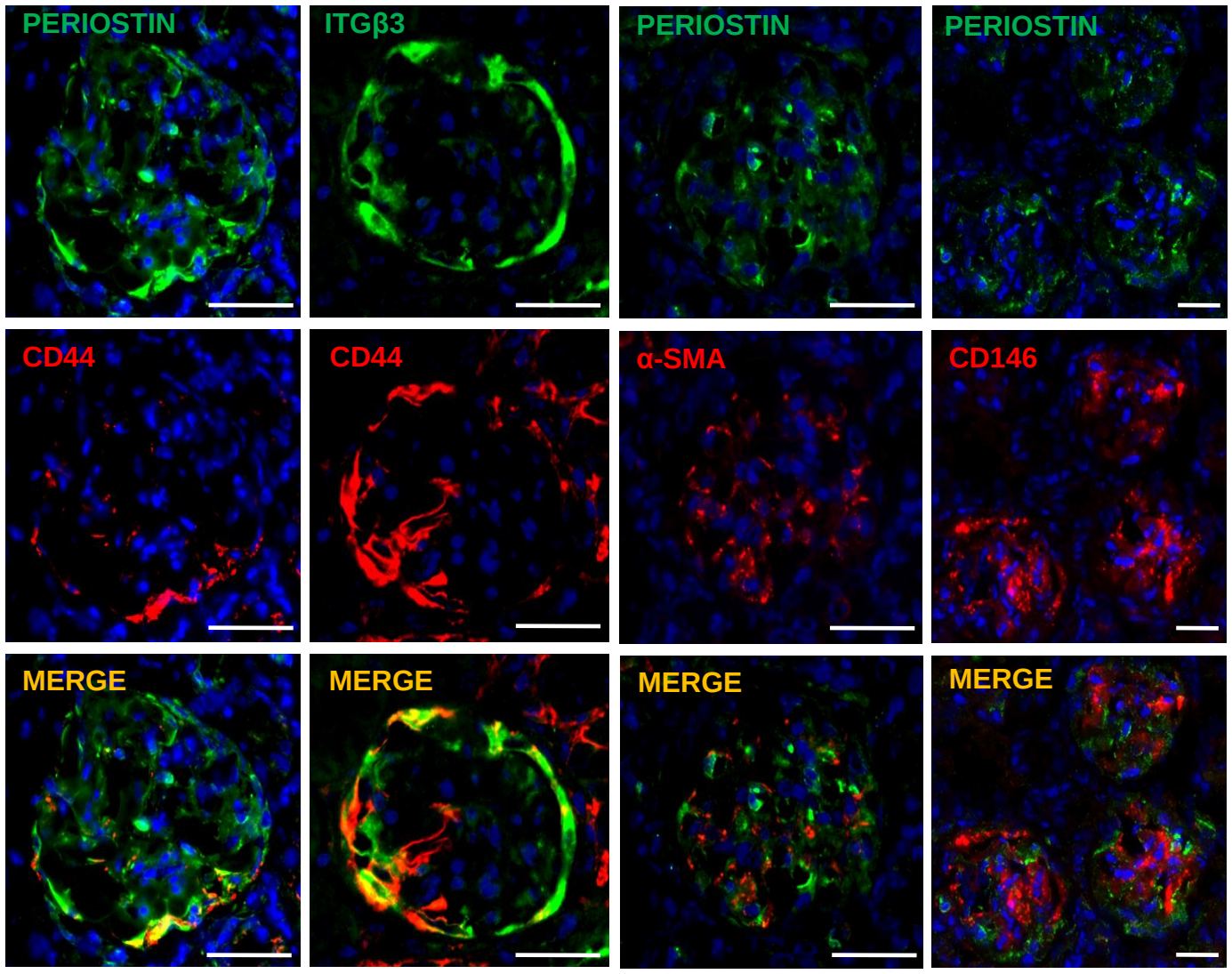

J

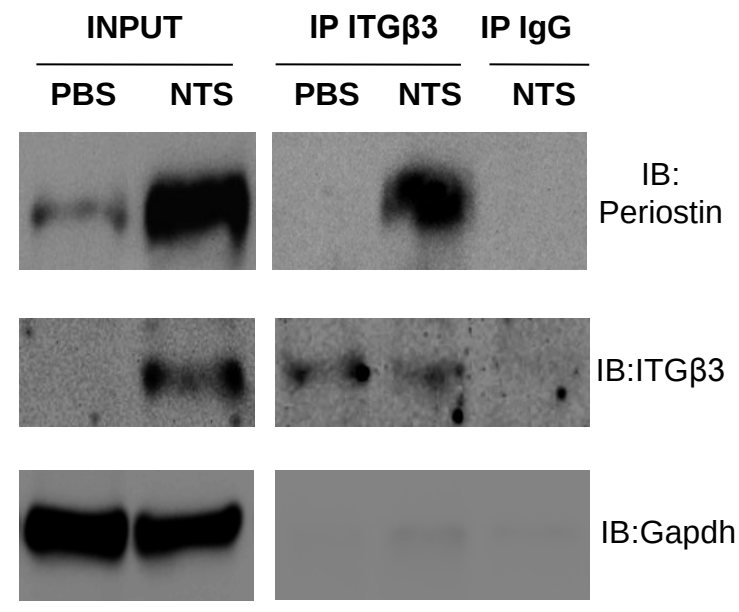

Figure 5

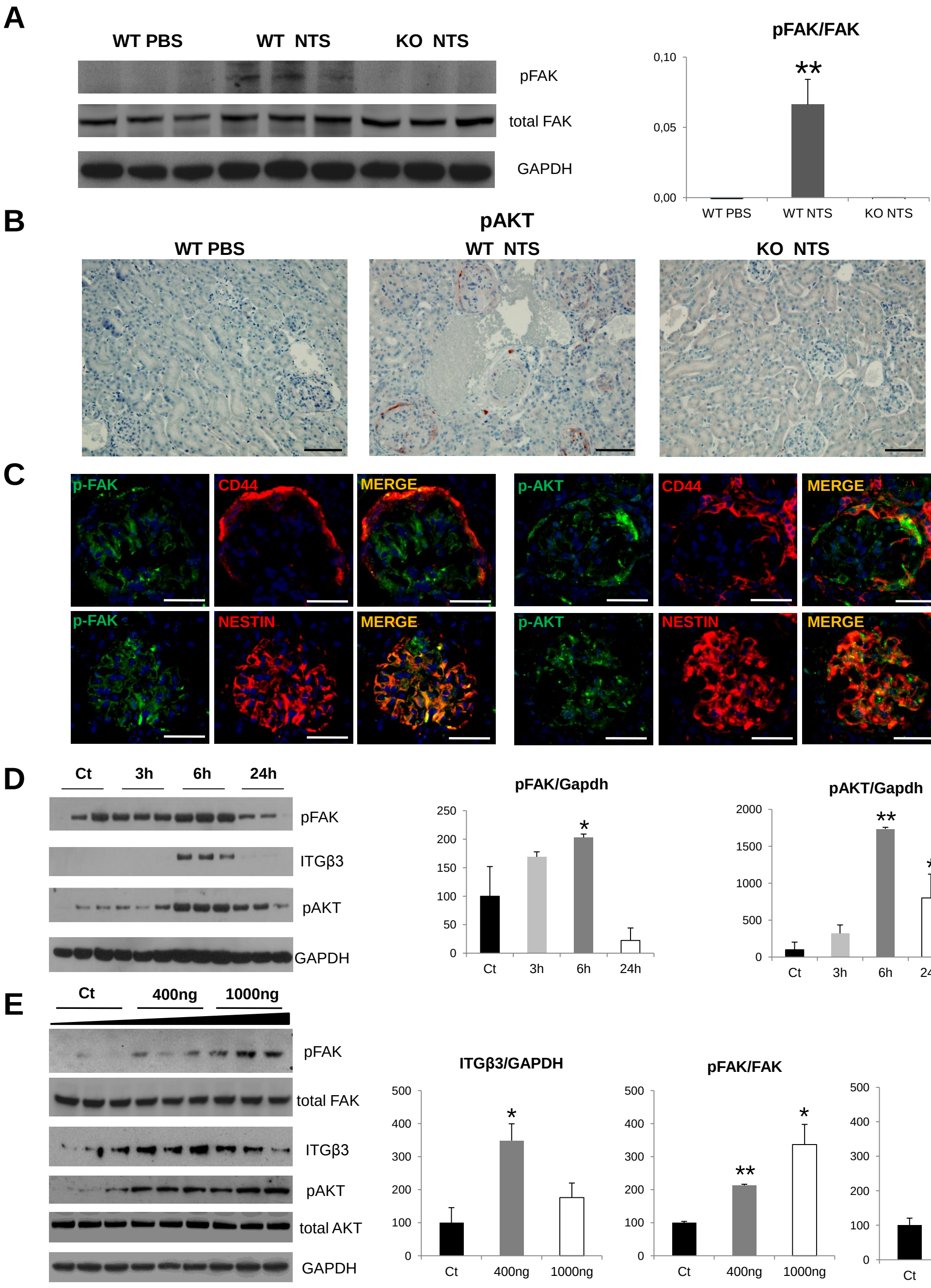
A
WT PBS
WT NTS
KO NTS
pFAK
total FAK
GAPDH
pFAK/FAK
0,10
0,05
0,00
**
WT PBS
WT NTS
KO NTS
B
pAKT
WT PBS
WT NTS
KO NTS
C
p-FAK
CD44
MERGE
p-AKT
CD44
MERGE
p-FAK
NESTIN
MERGE
p-AKT
NESTIN
MERGE
D
Ct
3h
6h
24h
pFAK
ITGβ3
pAKT
GAPDH
pFAK/Gapdh
250
200
150
100
50
0
*
Ct
3h
6h
24h
pAKT/Gapdh
2000
1500
1000
500
0
**
*
Ct
3h
6h
24h
E
Ct
400ng
1000ng
pFAK
total FAK
ITGβ3
pAKT
total AKT
GAPDH
ITGβ3/GAPDH
500
400
300
200
100
0
*
Ct
400ng
1000ng
pFAK/FAK
500
400
300
200
100
0
**
*
Ct
400ng
1000ng
pAKT/AKT
500
400
300
200
100
0
**
*
Ct
400ng
1000ng

Figure 6

A

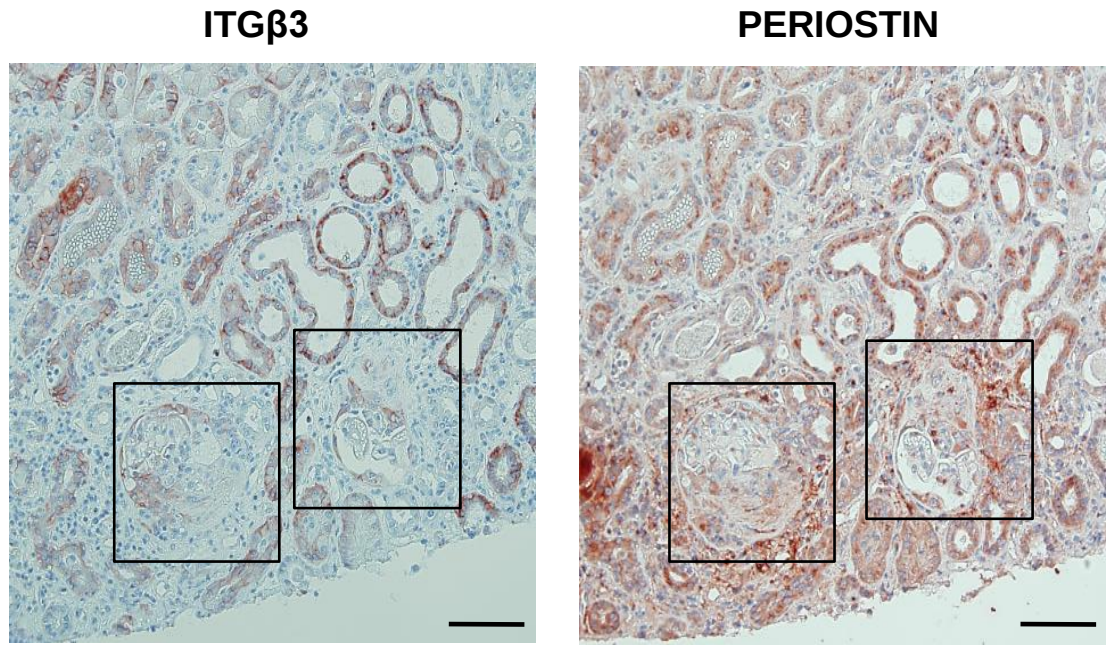

B

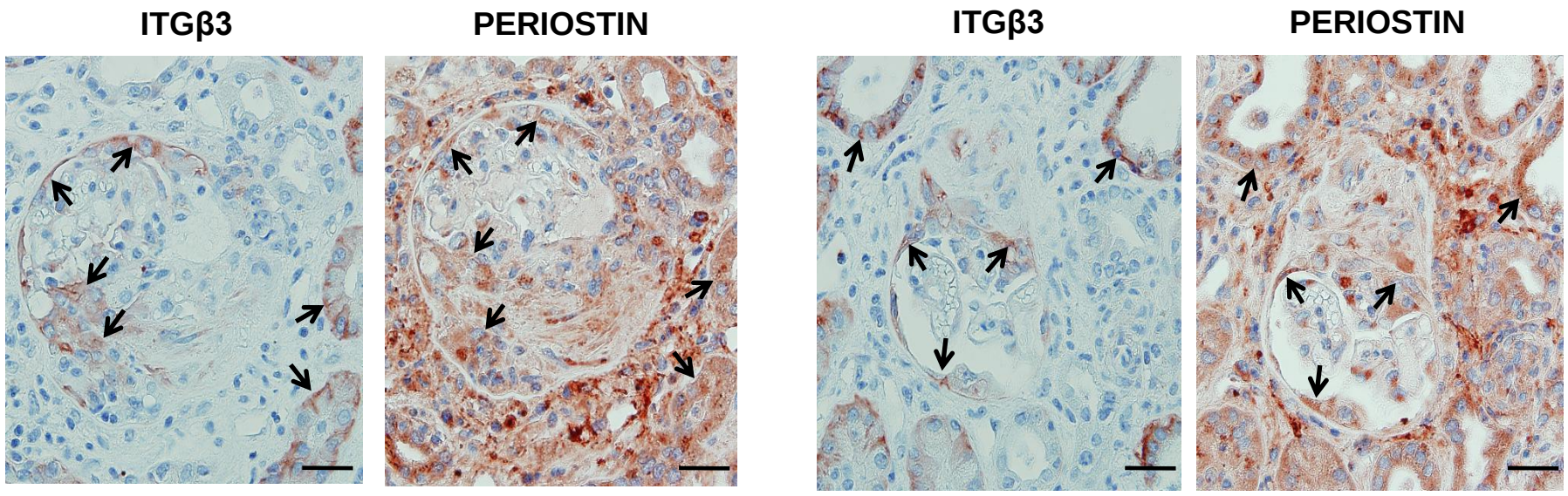

Figure 7

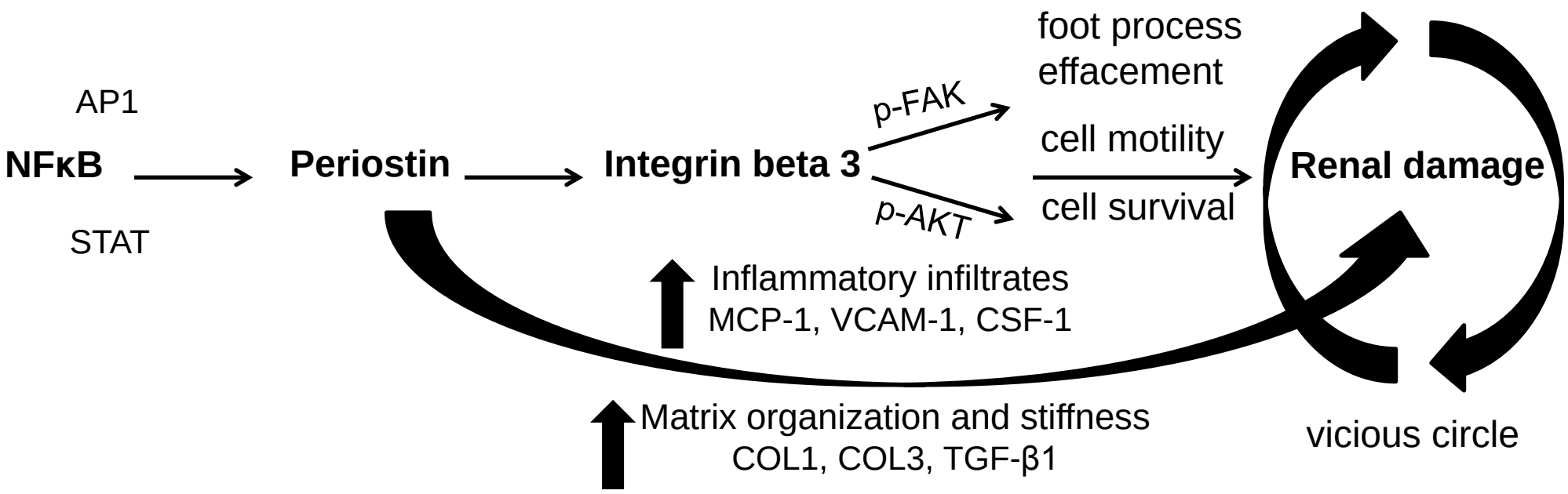
AP1
NFκB
STAT
Periostin
Integrin beta 3
p-FAK
p-AKT
foot process effacement
cell motility
cell survival
Renal damage
Inflammatory infiltrates
MCP-1, VCAM-1, CSF-1
Matrix organization and stiffness
COL1, COL3, TGF-β1
vicious circle

Supplemental Methods

Thioglycolate peritonitis and analysis of isolated macrophages

White blood cell analysis of peripheral blood was performed using a MS9V5 apparatus (MELET SCHLOESING Laboratoires, Osny, France).

For isolation of activated primary monocytes/macrophages, thioglycolate peritonitis was induced in periostin WT and KO littermates (C57BL/6) after intra-peritoneal injection of 1ml sterile 4% thioglycolate solution (Sigma Aldrich). The mice were sacrificed 72 hours after injection and the peritoneal cavities were washed twice with 5ml sterile PBS in order to collect the infiltrated monocytes/macrophages. Monocyte cell counts were performed in a Neubauer hemocytometer and expressed as total number of isolated cells.

For migration assays, $2x10^4$ peritoneal monocytes/macrophages diluted in RPMI 1640 medium were placed in the upper chambers of 48-well 5μm-pore Transwell chemotaxis supports (Corning Inc). 100ng/ml mouse recombinant monocyte chemattractant protein-1 (MCP-1) (R&D Systems) diluted in RPMI 1640 medium was added in the lower chambers. After incubation at 37ºC/5% CO_2 for 3 hours, the cells migrated in the lower chamber were fixed in 4% Parafolmadehyde (PFA) and counted under a microscope. The results were expressed as total number of cells migrated in the lower chamber.

For quantitative RT-PCR analysis, total RNA was extracted from peritoneal monocytes/macrophages using the EZ-10 Spin Column Total RNA Mini-preps Super kit (Bio Basic Inc) and transcribed to cDNA followed by Real-time PCR analysis as described in Concise Methods.

n=5-6 per group.

Supplemental figures and figure legends

Fold change of Itgβ3 and Postn in several nephropathies

Dataset	Reich IgA nephropathy (vs. healthy donor)	Rodwell Aging (anormal vs. normal proteinuria)	Schmid Diabetes (vs. Minimal Change Disease)	Woroniecka Diabetes (vs. healthy donor)	Berthier Lupus			Hodgin FSGS (vs. normal kidney)
Subcategory					Class II vs. Class III	Nephrotic vs. Subnephrotic	Class II vs. Class IV	
ITGB3 (Fold Change)	1,5 **	1,29 *	1,25 **	1,8 ***	1,27 **	1,97 **	1,14 *	1,31 *
POSTN (Fold Change)	1,57 **	2,03 *	2,02 *	5,23 **	2,36 *	3,87 ***	2,48 *	1,93 *

Dataset	Neusser Hypertension (Nephrosclerosis vs. Tumor nephrectomy)	Nakagawa CKD (vs. normal kidney)		Ju CKD 2					
Subcategory		Validation Set	Discovery Set	Vasculitis vs. Healthy Donor	IgA nephropathy vs. Healthy Donor	FSGS vs. Healthy Donor	Lupus Nephritis vs. Healthy Donor	Membranous Nephropathy vs. Healthy Donor	Minimal Change Disease vs. Healthy Donor
ITGB3 (Fold Change)	1,27 *	5,99 **	2,06 ***	1,44 ***	1,15 *	1,2 *	1,14 **	Not significant	Not significant
POSTN (Fold Change)	2,32 **	3,12 *	1,56 **	2,12 ***	1,31 *	1,29 *	1,59 **	Not significant	Not significant

Supplemental Figure 1. Comparison of the gene expression profiles of periostin (Postn) and integrin-β3 (Itgβ3) in different renal disease datasets as deposited in the publicly available Nephroseq platform (www.nephroseq.org). Postn and Itgβ3 are significantly up-regulated to a comparable level in several categories of renal disease patients. **P*<0.05, ***P* <0.01, ****P*<0.001 vs. respective control.

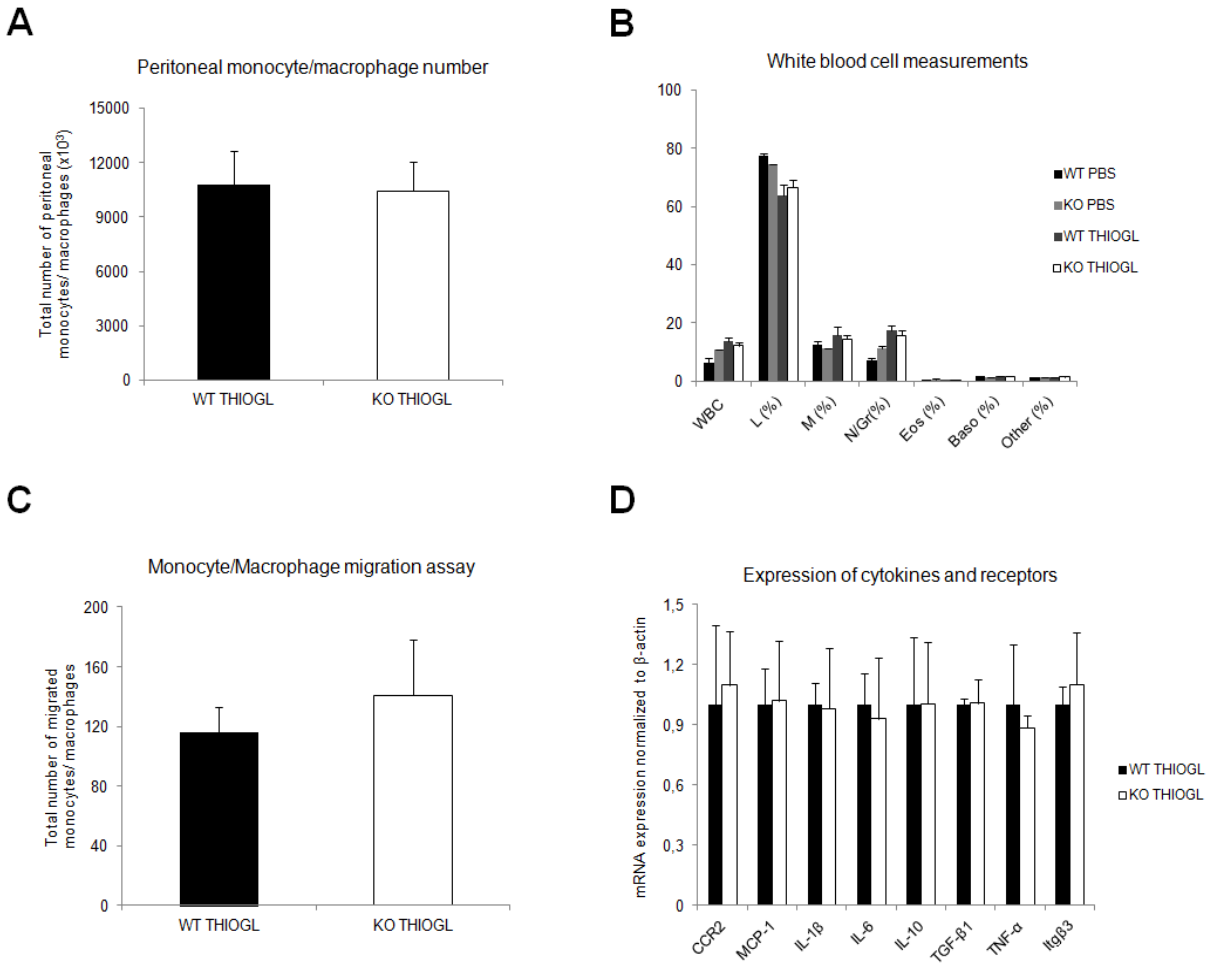

Supplemental Figure 2. Comparative phenotypic analysis of activated monocytes isolated after thioglycolate-induced peritonitis did not reveal any differences between WT and KO mice. (A) The total number of infiltrated peritoneal monocytes/macrophages was similar in WT and KO mice. (B) White blood cell analysis of peripheral blood before and after thioglycolate treatment did not reveal any variations in the leukocyte subtypes between WT and KO mice. (C) Isolated peritoneal monocytes/macrophages from WT and KO mice were left to migrate towards chemoattractant protein MCP-1 in Transwell chambers for 3hr at 37ºC, before measurement of the total number of migrated cells in the lower chamber. Macrophages from both WT and KO mice showed the same migratory capacities. (D) Quantitative RT-PCR analysis of various cytokines/receptors in isolated peritoneal

monocytes/macrophages from WT and KO mice did not show any differences between groups. Total monocyte/macrophage number is in millions (x 10^3) (A). Total WBC number is in thousands/mm^3 (x $10^3/mm^3$), while subtypes are in percentage of total cells (%). L=lymphocytes, M=monocytes, N/Gr=neutrophils, Eos=eosinophils, Baso=basophiles (B). *n*=5-6 per group.

Supplemental Tables

ODN	Sequence
AS1	G*A*G*AGGAACCATCTTCAGCCCTGAGCT*C*C*G
AS2	G*T*C*TCTCCTGTTTCTCC*A*C*C
SCR1	C*T*C*TCCGGAGAGCCACCGAGATCTGAG*T*C*A
SCR2	G*C*T*ATCCTTCCCGCTCT*C*T*T

Supplemental Table 1. SCR and AS ODN sequences used for *in vivo* administration in mice. *Residues modified with phosphorothioates to inhibit degradation.

Target mRNA	Forward	Reverse
COL1	GCAGGTTCACCTACTCTGTCCT	CTTGCCCCATTCATTTGTCT
COL3	TGGTTTCTTCTCACCCTTCTTC	TGCATCCCAATTCATCTACGT
TGF-β1	TGGAGCAACATGTGGAACTC	GTCAGCAGCCGGTTACCA
MCP-1	CATCCACGTGTTGGCTCA	GATCATCTTGCTGGTGAATGAGT
RANTES	CTACTCCCACTCCGGTCCT	GATTTCTTGGGTTTCGTGGTC
VCAM-1	TGGTGAAATGGAATCTGAACC	CCCAGATGGTGGTTTCCTT
CSF-1	CAGCTGCTTCACCAAGGACT	TCATGGAAAGTTCGGACACA
ITGβ3	GTGGGAGGGCAGTCCTCTA	CAGGATATCAGGACCCTTGG
mPOSTN	CGGGAAGAACGAATCATTACA	ACCTTGGAGACCTCTTTTTGC
hPOSTN	GAACCAAAAATTAAAGTGATTGAAGG	TGACTTTTGTTAGTGTGGGTCCT

Supplemental Table 2. Primer sequences used in quantitative real-time PCR analysis to detect target mRNA expression.

Position on periostin promoter	Forward primer	Reverse primer
-2100-2000	AAACTGCCTTCCTTTTCTCAGC	GAGAAACAGAGGCCAGGTCAGA
-1450-1300	CACAAGTGCCCTGGAAGGAA	ACACAGCCAAACAACACAGT
-1100-950	TGCCTTGTCAGTGGGAAAACA	GCAAGGAATGGAAACAGCCAT
-950-800	CCATTCCTTGCCAACTGAAGC	CTCAGCATTCTTAGCTGAGGGA
-750-650	CTCTTGGCAGCAACCCTGTT	ACACACACACTGCATACTCTGAT
-500-300	GTTGAAAAGACATGGCCCCAG	ATCACTCCACAGCAGAACACG
-250-100	GTGCAATCAGATCAAACCAGGA	TTCAATCATGGTGAGCCCGTTT
-50+100	CCACAGCCCAGAGCTATATAAAC	TAACTGTTGGCATTTGCAGGG

Supplemental Table 3. Primer sequences used in quantitative real-time PCR analysis to detect enrichment of mouse periostin promoter fragments in ChIP assays.